


RESEARCH ARTICLE

Bacteroides fragilis expresses three proteins similar to *Porphyromonas gingivalis* HmuY: Hemophore-like proteins differentially evolved to participate in heme acquisition in oral and gut microbiomes

Svetlana V. Antonyuk¹ | Klaudia Siemińska² | Michał Śmiga² | Richard W. Strange³ | Mateusz Wagner² | Katie J. Barnett¹ | Teresa Olczak² 

¹Molecular Biophysics Group, Institute of Systems, Molecular and Integrative Biology, Faculty of Health and Life Sciences, University of Liverpool, Liverpool, UK

²Laboratory of Medical Biology, Faculty of Biotechnology, University of Wrocław, Wrocław, Poland

³School of Life Sciences, University of Essex, Colchester, UK

Correspondence

Teresa Olczak, Laboratory of Medical Biology, Faculty of Biotechnology, University of Wrocław, Wrocław, Poland
Email: teresa.olczak@uwr.edu.pl

Svetlana V. Antonyuk, Molecular Biophysics Group, Institute of Systems, Molecular and Integrative Biology, Faculty of Health and Life Sciences, University of Liverpool, Liverpool, UK
Email: s.antonyuk@liverpool.ac.uk

Present address

Mateusz Wagner, Department of Molecular Biology and Genetics, Weill Institute for Cell and Molecular Biology, Cornell University, Ithaca, NY, USA

Abstract

Oral and gut microbiomes are important for the maintenance of homeostasis in the human body. Altered or disturbed mutualism between their members results in dysbiosis with local injury and subsequent systemic diseases. The high bacterial density causes intense competition among microbiome residents to acquire nutrients, including iron and heme, the latter of high importance for heme auxotrophic members of the Bacteroidetes phylum. Our main hypothesis is that the heme acquisition mechanism, with the leading role played by a novel HmuY family of hemophore-like proteins, can be used to fulfill nutritional requirements and increase virulence. We characterized HmuY homologs expressed by *Bacteroides fragilis* and compared their properties with the first representative of this family, the HmuY protein of *Porphyromonas gingivalis*. In contrast to other Bacteroidetes members, *B. fragilis* produces three HmuY homologs (Bfr proteins). All *bfr* transcripts were produced at higher levels in bacteria starved of iron and heme (fold change increase ~60, ~90, and ~70 for *bfrA*, *bfrB*, and *bfrC*, respectively). X-ray protein crystallography showed that *B. fragilis* Bfr proteins are structurally

Abbreviations: ABA, anaerobic blood agar plates; BHI, brain-heart infusion medium; BHIS, BHI supplemented with heme; CBB, Coomassie Brilliant Blue; CPIII, coproporphyrin III; DIP, dipyriddy; DM, minimal medium; DSF, differential scanning fluorimetry; FBS, fetal bovine serum; Fe(II/III)PPIX, heme (protoheme); FeDPPIX, deuteroheme; FeMPPIX, mesoheme; HSA, human serum albumin; MD, molecular dynamics simulations; OD, optical density; OMV, outer membrane vesicles; PBS, phosphate-buffered saline; PPIX, protoporphyrin IX; RT-qPCR, reverse transcriptase-quantitative polymerase chain reaction; SDS-PAGE, sodium dodecyl sulfate-polyacrylamide gel electrophoresis; TBS, Tris buffer.

Svetlana V. Antonyuk, Klaudia Siemińska, Michał Śmiga contributed equally to this work and are listed alphabetically.

This is an open access article under the terms of the [Creative Commons Attribution-NonCommercial-NoDerivs](https://creativecommons.org/licenses/by-nc-nd/4.0/) License, which permits use and distribution in any medium, provided the original work is properly cited, the use is non-commercial and no modifications or adaptations are made.

© 2023 The Authors. *The FASEB Journal* published by Wiley Periodicals LLC on behalf of Federation of American Societies for Experimental Biology.

Funding information

National Science Center (Narodowe Centrum Nauki, Krakow, Poland), Grant/Award Number: 2019/33/B/NZ6/00292; The University of Liverpool BAG, Grant/Award Number: mx21970

similar to *P. gingivalis* HmuY and to other homologs, except for differences in the potential heme-binding pockets. BfrA binds heme, mesoheme, and deuteroheme, but preferentially under reducing conditions, using Met175 and Met146 to coordinate heme iron. BfrB binds iron-free protoporphyrin IX and coproporphyrin III, whereas BfrC does not bind porphyrins. HmuY is capable of heme sequestration from BfrA, which might increase the ability of *P. gingivalis* to cause dysbiosis also in the gut microbiome.

KEYWORDS

Bacteroides fragilis, Bacteroidetes phylum, heme, heme-binding protein, hemophore-like protein, HmuY, microbiome, *Porphyromonas gingivalis*

1 | INTRODUCTION

Data obtained from the MetaHIT (the European Metagenomics of the Human Intestinal Tract Project; <http://www.metahit.eu>), the NIH Human Microbiome Project (<http://hmpdacc.org>), and the AsianGut Microbiome Project (<http://www.asiangut.com>) have revealed high diversity of the human microbiome, as well as the possibility of mouth-gut transmission of some species. Both oral and gut microbiomes are important for the maintenance of homeostasis in the human body and for maintaining epithelial barrier integrity. However, altered or disturbed mutualism between microbiota results in dysbiosis with local injury and subsequent systemic diseases.^{1–4}

The Bacteroidetes, one of the dominant phyla of bacteria composing a significant fraction of the gut microbiome, can be both commensal and opportunistic.^{5,6} They are important for maintaining the immune balance in the human body and for protection from inflammatory diseases.⁷ In contrast to *Bacteroides vulgatus* and *Bacteroides thetaiotaomicron*, *Bacteroides fragilis* is one of the least abundant *Bacteroides* species in the gut, but it is the most common bacterium identified in anaerobic infections, with a high mortality rate.^{8–10} Disruption of the mucosal surface of the gut by inflammation, neoplastic tumor, or surgery, and subsequent spread of *B. fragilis* to the blood or surrounding tissues, results in clinically significant intra-abdominal infections, abscess formation, endocarditis, and pericarditis, often resulting in sepsis, organ failure, and death.^{10–12} Another member of the Bacteroidetes phylum, *Porphyromonas gingivalis*, is a keystone etiologic agent of periodontal diseases.^{13–15} This pathogen is not only responsible for dysbiosis in the oral cavity, leading to the destruction of tooth-supporting tissues, but importantly, it has been demonstrated to be engaged in the onset and progression of several systemic diseases.^{16–22}

Recent studies showed that mouth-gut bacterial transmission and invasion of the gut by *P. gingivalis* are also able to influence the outcome of various diseases such as colitis and bowel disease.^{23–31} In mouse model studies, orally administered *P. gingivalis* invaded the gastrointestinal tract, changed the gut bacterial composition, and lowered the complexity of the gut microbiota.^{29–35} *P. gingivalis* also led to increased permeability of the gut epithelium and endotoxemia, which in turn caused not only local inflammation, but importantly systemic inflammation.^{21,25,26,28,29,33,35–38} Several studies showed the association between periodontitis and inflammatory bowel disease and demonstrated that *P. gingivalis* not only enhanced mucosal damage in mice with experimentally induced colitis,³⁹ but was significantly more abundant in patients with ulcerative colitis or Crohn's disease.^{36,38–42}

The high bacterial density in the gut causes intense competition among microbiome residents in their acquisition of nutrients, including iron and heme. The heme dependence of several auxotrophic Bacteroidetes members is due to their inability to synthesize precursors of protoporphyrin IX (PPIX). Some Bacteroidetes, including *P. gingivalis* and *B. fragilis*, are able to synthesize heme in vitro if PPIX and inorganic iron are supplied.^{43–48} *Bacteroides* and *Porphyromonas* species can also remove non-iron metals from metalloporphyrins.^{46–50} After dechelation, ferrous iron can be inserted into the metal-free porphyrin through a ferrochelatase activity to form heme (FePPIX), and also, in the case of *B. fragilis*, mesoheme (FeMPIX) or deuteroheme (FeDPIX). *B. fragilis* is able to act on and modify labile heme molecules in vitro⁴⁶ and can grow in and incorporate mesoheme and deuteroheme into a functional *b*-type cytochrome.⁵¹ It has been suggested that chelatase/dechelataase activity could be performed by *P. gingivalis* HmuS protein^{46,48,52–55} or homologous *B. fragilis* BtuS2 protein,⁴⁶ both encoded on the *hmu* operon or *hmu*-like gene clusters, respectively. A recent study demonstrated

that the abilities of *B. fragilis* to utilize heme or PPIX for growth, as well as intestinal colonization and intra-abdominal infection, were reduced in the mutant lacking a *uroS* gene, which was linked with the suppression of chelate/dechelate activity.⁵⁶ In contrast to *P. gingivalis*, to acquire iron, *B. thetaiotaomicron* and *B. vulgatus* can utilize Fe(III)-enterobactin and Fe(III)-salmochelin S4, whereas *B. fragilis* can utilize Fe(III)-ferrichrome, all of which are xenosiderophores produced by enterobacteria.^{47,57,58} After transporting heme or siderophore through the outer membrane of *B. fragilis* or *P. gingivalis*, respectively, iron is internalized by the inner-membrane ferrous iron transporter system (FeoAB).^{46,59}

A factor that plays an important role in survival of *B. fragilis* in extraintestinal infection is its ability to acquire heme from host tissues.^{60,61} Although *B. fragilis* proteins involved in heme acquisition have been reported, including an iron-repressible 44-kDa outer membrane heme-binding protein (HupA) and hemolysins HlyA, HlyB, and HlyIII,^{62–67} knowledge regarding the mechanisms involved in this process is still limited. In comparison with *B. fragilis*, the heme acquisition mechanisms of *P. gingivalis* are much better characterized. Among them is a heme utilization system (Hmu system), with the leading role played by the hemophore-like protein HmuY, used to sequester heme from host hemoproteins and deliver it to the TonB-dependent outer membrane receptor HmuR for subsequent heme transport through the outer membrane.⁶⁸ Our analyses have led us to the finding that *P. gingivalis* displays a novel heme acquisition mechanism, whereby oxyhemoglobin is firstly oxidized to methemoglobin, which enables more efficient heme sequestration by *P. gingivalis* HmuY. Generation of methemoglobin involves the arginine-specific gingipain protease A (RgpA) produced by *P. gingivalis*,⁶⁹ the interpain A (InpA) protease produced by *P. intermedia*,⁷⁰ or H₂O₂ produced by *Streptococcus gordonii*.⁷¹ Interestingly, we have also demonstrated that the presence of *Pseudomonas aeruginosa* pyocyanin facilitates the extraction of heme from hemoglobin by the *P. gingivalis* HmuY by rapidly oxidizing oxyhemoglobin to methemoglobin.⁷² HmuY is also able to compete with albumin for heme,⁶⁹ as well as sequester heme from hemopexin.⁷³ We also demonstrated that a housekeeping protein, exhibiting a moonlighting function, namely, glyceraldehyde-3-phosphate dehydrogenase (SgGAPDH), produced by *Streptococcus gordonii*, as well as HmuY homologs produced by other periodontopathogens, may bind heme and then serve as heme donors for *P. gingivalis*.^{73–76} Therefore, our novel paradigm of heme acquisition, which is displayed by the black-pigmented anaerobes, appears to extend to co-infections with other bacteria and offers a synergistic mechanism for the ability of *P. gingivalis* to obtain sufficient heme in the host

environment. These findings have been supported by studies demonstrating that *P. gingivalis* HmuY is required for the bacterial survival and invasion of human cells not only *in vitro*,⁷⁷ but importantly, its significantly higher expression in patients with periodontitis would confirm its requirement under *in vivo* conditions.^{78–80}

Previously, we identified the presence of, and characterized, HmuY homologs in other periodontopathogens belonging to the Bacteroidetes phylum, namely, in *Tannerella forsythia* (Tfo)⁷³ and in *Prevotella intermedia* (PinO and PinA),⁷⁴ as well as in *Bacteroides vulgatus* (Bvu).⁷⁶ Our main hypothesis is that the heme acquisition mechanism, with the leading role played by the novel HmuY family of hemophore-like proteins expressed by members of the Bacteroidetes phylum, can be used to fulfill their nutritional requirements and increase their virulence. Importantly, differences in heme-binding modes and heme sequestration ability between *P. gingivalis* HmuY and its homologs expressed not only by cohabitating periodontopathogens but also by gut bacteria, may provide *P. gingivalis* with heme, thus increasing its tendency to cause dysbiosis in both the oral and gut microbiomes. Therefore, the aim of this study was to characterize three potential HmuY homologs expressed by *B. fragilis* and compare their properties with *P. gingivalis* HmuY.

2 | MATERIALS AND METHODS

2.1 | Bacterial stains and growth conditions

P. gingivalis A7436, *B. fragilis* NCTC 9343 (ATCC 25285; Pol-Aura, Olsztyn, Poland), and *B. fragilis* 638R (Institute Pasteur, Paris, France) were grown anaerobically (Whitley A35 anaerobic workstation; Bingley, UK) at 37°C for 5 days on blood agar plates (ABA) composed of Schaedler broth (containing hemin and L-cysteine), and supplemented with 5% sheep blood and menadione (Biomaxima, Lublin, Poland).

P. gingivalis colonies were inoculated into liquid basal medium (BM) prepared with 3% trypticase soy broth (Becton Dickinson, Sparks, MD, USA), 0.5% yeast extract (Biomaxima), 0.5 mg/L menadione (Fluka, Munich, Germany), 0.05% L-cysteine (Sigma-Aldrich, St. Louis, MO, USA), and 7.7 μM hemin (Pol-Aura).

B. fragilis colonies were inoculated into liquid brain-heart infusion medium (BHI), supplemented with 10 μg/mL heme (Pol-Aura), 0.2% NaHCO₃ (Sigma-Aldrich), and 1 g/L cysteine (Sigma-Aldrich) (heme-supplemented BHI medium; BHIS), or into minimal medium (DM) composed of 1.5 g/L KH₂PO₄ (Sigma-Aldrich), 0.5 g/L NH₄SO₄ (Sigma-Aldrich), 0.9 g/L NaCl (Sigma-Aldrich),

150 mg/L L-methionine (Sigma-Aldrich), 5 µg/L vitamin B₁₂ (Sigma-Aldrich), 20 mg/L MgCl₂ × 6H₂O (Sigma-Aldrich), 10 mg/L CaCl₂ × 2H₂O (Sigma-Aldrich), 1 mg/L MnCl₂ × 4H₂O (Sigma-Aldrich), 1 mg/L CoCl₂ × 6H₂O (Sigma-Aldrich), 1 mg/L resazurin (Sigma-Aldrich), 1 g/L L-cysteine (Sigma-Aldrich), 5 g/L glucose (Sigma-Aldrich), 1 g/L tryptone (Biomaxima), and 20 mL of 10% NaHCO₃ (Sigma-Aldrich) per liter (final pH 7.2). To analyze *B. fragilis* gene expression, bacteria were grown in iron/heme-rich conditions (BHIS) and either inoculated into BHIS or DM supplemented with various concentrations of selected compounds (heme, PPIX, dipyr- idyl [DIP]) and cultured for 24 h or starved of iron and heme (DM without added heme and supplemented with 160 µM DIP) for 24 h and then inoculated into DM supplemented with various concentrations of selected compounds (hemoglobin, heme, PPIX, DIP) and cultured for 24 h.

To monitor the influence of heme, PPIX, or coproporphyrin III (CPIII) on the growth of *B. fragilis*, bacteria were cultured for two passages in BHI medium, supplemented with 0.2% NaHCO₃, 1 g/L cysteine, and 160 µM DIP. Then, 200 µL of fresh BHI medium, supplemented with 0.2% NaHCO₃ and 1 g/L cysteine, and additionally supplemented with various concentrations of ammonium iron(II) sulfate (Sigma-Aldrich) and/or hemin chloride, or PPIX, or CPIII, were inoculated with bacteria at a starting optical density at 600 nm (OD₆₀₀) equal to 0.2. Growth curves were measured using a Stratus plate reader (Cerrillo, Charlottesville, VA, USA) every 1 h for 24 h.

Escherichia coli BL21-CodonPlus-RIL (Agilent Technologies, Santa Clara, CA, USA) and DH10β (New England Biolabs, Ipswich, MA, USA) strains were cultured under standard aerobic conditions.

2.2 | Site-directed mutagenesis, overexpression, and purification of proteins

The modified pMAL-c5x_His plasmid constructed in our previous study⁸¹ was used to clone DNA sequences (amplified by PCR using isolated genomic DNA) encoding *B. fragilis* BfrA (GenBank locus ID: CAH08403), BfrB (GenBank locus ID: CAH06766), and BfrC (GenBank locus ID: CAH07859) proteins, lacking the predicted signal peptides (MRKAILFCLAITLLGTM LISFSACN, MNNKN KFRFAILLFGVLSAFITAC, MKHTGLFKTLFCAGCL LLSAC, respectively). All proteins were overexpressed in *E. coli* BL21-CodonPlus-RIL cells (Agilent Technologies) and purified from soluble fractions obtained from *E. coli* cell lysates, and the fusion tag was removed from purified recombinant proteins as described previously.^{73,74} All

primers used in this study are listed in Table S1. HmuY and HusA proteins were overexpressed and purified as described previously.⁸² Concentration of the purified proteins was determined spectrophotometrically using the empirical molar absorption coefficients determined for apo-forms of BfrA ($\epsilon_{280\text{nm}} = 42.81 \text{ mM}^{-1} \text{ cm}^{-1}$), BfrB ($\epsilon_{280\text{nm}} = 25.08 \text{ mM}^{-1} \text{ cm}^{-1}$), and BfrC ($\epsilon_{280\text{nm}} = 63.57 \text{ mM}^{-1} \text{ cm}^{-1}$) in this study, and for HmuY ($\epsilon_{280\text{nm}} = 36.86 \text{ mM}^{-1} \text{ cm}^{-1}$) and HusA ($\epsilon_{280\text{nm}} = 33.81 \text{ mM}^{-1} \text{ cm}^{-1}$) as reported previously.^{82,83}

Point mutations were introduced into the respective genes using a QuikChange II XL Site-Directed Mutagenesis Kit (Agilent Technologies). Selected amino acids with a potential ability to coordinate heme iron, chosen based on amino acid alignment and comparison of three-dimensional protein structures, were substituted by alanine, resulting in single-point mutations. Sequences of site-directed mutagenesis primers are available upon request.

2.3 | Protein-heme/protoporphyrin IX/coproporphyrin III complex formation and titration experiments

Heme (hemin chloride; Pol-aura, Olsztyn, Poland) solutions were prepared as reported previously.^{69,73} To analyze the redox properties of the heme iron, 10 mM of sodium dithionite prepared in PBS was used as the reductant, and 1 mM of potassium ferricyanide prepared in PBS as the oxidant.^{73,74,84} Deuteroheme (FeDPIX) and mesoheme (FeMPIX) (Frontier Specialty Chemicals, Logan, UT, USA) were prepared as described previously.^{85,86} PPIX (Sigma-Aldrich, St. Louis, MO, USA) stock solution was prepared by dissolving PPIX in pure DMSO (99.9%) (Fluka, Munich, Germany) and its concentration was determined in DMSO using the empirical molar absorption coefficient $\epsilon_{405\text{nm}} = 150 \text{ mM}^{-1} \text{ cm}^{-1}$.⁸⁷ CPIII (Frontier Scientific, Logan, UT, USA) stock solution was prepared by dissolving in 0.1 M NaOH and the concentration was determined in 50 mM HEPES pH 7.5,⁸⁸ using the empirical molar absorption coefficient $\epsilon_{393\text{nm}} = 150.74 \text{ mM}^{-1} \text{ cm}^{-1}$.

The formation of porphyrin-protein complexes was examined in 20 mM of sodium phosphate buffer, pH 7.4, containing 140 mM of NaCl (phosphate-buffered saline, PBS). UV-visible absorption spectra were recorded in the range 250–700 nm with a double beam Jasco V-750 spectrophotometer using cuvettes with 10 mm path length. Titration curves were analyzed using the equation for a one-site binding model, and dissociation constant (K_d) values were determined as reported earlier^{73,74} using OriginPro 8 software (OriginPro Corporation, Northampton, MA, USA).

2.4 | Size-exclusion chromatography

Analytical size-exclusion chromatography was carried out under air (oxidizing) and reducing conditions. Samples (0.8 mg, 400 μ L) in 50 mM Tris-HCl buffer, containing 140 mM NaCl, pH 7.4 (Tris buffer, TBS), were applied onto a Superdex 75 Increase 10/300 GL column (Sigma-Aldrich) connected to an ÄKTA Pure FPLC system (GE Healthcare, Chicago, IL, USA). To analyze proteins under reducing conditions, 30 mM of sodium dithionite was added to the separating buffer (TBS).

2.5 | Heme sequestration experiments

The albumin-heme complex was prepared by incubating a 120- μ M stock solution of human albumin (Sigma-Aldrich) in PBS at a 1:1.2 protein-to-heme molar ratio and subsequently passed through Zeba Spin Desalting Columns (Sigma-Aldrich) to ensure that no un-complexed heme remained. Human hemopexin (Sigma-Aldrich) was solubilized in PBS and incubated with heme as described above. Human methemoglobin (Sigma-Aldrich) was solubilized in PBS. The hemoproteins were incubated with *B. fragilis* proteins as described previously.⁷³ Co-incubation of HmuY with *B. fragilis* proteins was carried out in PBS and monitored by UV-visible spectroscopy under air (oxidizing) or reducing conditions, using each protein at 5- μ M concentration.⁷³

2.6 | Sodium dodecyl sulfate-polyacrylamide gel electrophoresis (SDS-PAGE) and Western blotting

For SDS-PAGE, samples were prepared and analyzed as reported previously.⁷³ Separated proteins were stained with Coomassie Brilliant Blue G-250 (CBB; Sigma-Aldrich). For immunoblotting, samples were separated by SDS-PAGE, transferred onto nitrocellulose membranes (Millipore, Billerica, MA, USA), probed with polyclonal rabbit antibodies raised against purified BfrA, BfrB, and BfrC proteins (ProteoGenix, Schiltigheim, France), and complexes formed were detected using HRP-conjugated anti-rabbit IgG antibodies (Sigma-Aldrich) and chemiluminescence staining (Perkin Elmer, Waltham, MA, USA).⁷³

2.7 | Determination of susceptibility of proteins to proteolytic digestion

To examine the susceptibility of the Bfr proteins to bacterial proteases, *P. gingivalis* and *B. fragilis* cells were grown

in rich iron/heme conditions (ensuring proper cell viability and efficient proteolytic activity) in the presence of added purified HmuY or Bfr proteins at a final concentration of 5 μ M.⁷³ All cultures (1 mL) were started at $OD_{600}=0.2$ for *P. gingivalis* and $OD_{600}=0.4$ for *B. fragilis* and collected at 0-, 6-, and 24-h time points. The number of bacterial cells at the starting point was $\sim 2 \times 10^8$ or $\sim 4 \times 10^8$ per 1 mL of the culture medium for *P. gingivalis* and *B. fragilis*, respectively, and increased during cultivation. As controls, *P. gingivalis* or *B. fragilis* cultures without addition of the purified proteins or culture medium alone supplemented with proteins were analyzed. At the indicated time points, aliquots of samples were examined by SDS-PAGE and CBB staining.

2.8 | Bacterial cell fractionation

Portions of bacterial cultures were centrifuged at $4000 \times g$ for 20 min at 4°C and supernatants were filtered using sterile 0.22 μ m filters (Roth, Frederikssund, Denmark) to separate the cell-free culture supernatant and cells. To separate OMV, the filtered supernatants were concentrated using Amicon Ultra-4 Centrifugal Ultracel-100KDa filter units (Millipore) and ultracentrifuged at $100\,000 \times g$ for 2 h at 4°C using a Beckman fixed-angle rotor (Type 70 Ti; Beckman Coulter, Indianapolis, IN, USA). To examine soluble proteins, the culture supernatant was concentrated 25 \times with Amicon Ultra-4 Centrifugal Ultracel-10KDa filter units (Millipore). The cell pellet was washed twice with PBS and used to analyze the whole cell fraction.

2.9 | Reverse transcriptase-quantitative polymerase chain reaction (RT-qPCR)

RNA was purified from 0.5×10^8 – 4×10^8 *B. fragilis* cells as described previously.^{73,74} Reverse transcription was carried out with 200 ng of RNA using a LunaScript RT SuperMix Kit (New England Biolabs). PCR was performed using a SensiFAST SYBR No-ROX Kit (Bioline) and the LightCycler 96 System (Roche, Basel, Switzerland). The amplification reaction was carried out as follows: initial denaturation at 95°C for 2 min, 40 cycles of denaturation at 95°C for 5 s, primer annealing at 60°C for 10 s, and extension at 72°C for 20 s. The melting curves were analyzed to monitor the quality of PCR products. Relative quantification of the respective *bfr* gene expression was determined in comparison with the *16S rRNA* gene's expression (GenBank locus ID: BF638R_rRNA0004) as a reference, using the $\Delta\Delta C_t$ method and LightCycler 96 software (Roche). All

samples and controls were run in triplicate in three independent experiments for the target and reference genes. All primers are listed in Table S1.

2.10 | Differential scanning fluorimetry (DSF)

To determine conformational stability of the purified proteins, thermal unfolding and refolding were examined. Samples comprising proteins in apo-form or proteins with added heme were prepared in PBS and examined using a label-free fluorimetric analysis with Prometheus NT.48 apparatus (Nano Temper Technologies, Munich, Germany). NanoDSF grade capillaries were filled with 1 mg/mL protein solutions and heated from 25 to 90°C with a 1°C/min heating rate at low detector sensitivity with an excitation power of 8%. Unfolding and refolding transition points (T_m) were determined from the first derivative of the changes in the emission wavelengths of tryptophan and tyrosine fluorescence at 330 nm and 350 nm, respectively, automatically identified by the Prometheus NT.48 control software (Nano Temper Technologies). Two independent measurements were performed.

2.11 | Protein crystallization, X-ray data collection, processing, and structure determination

Both BfrB and BfrC proteins were crystallized by the hanging drop method at room temperature. For crystallization of BfrB, 2 μ L of 10 mg/mL protein (in 20 mM Tris/HCl, pH 7.5) was mixed with 2 μ L of reservoir solution, containing 2.6 M of ammonium sulfate and 100 mM of acetate buffer, pH 5.5, and equilibrated over 400 μ L of reservoir solution. Thin plates appeared within a few days. Crystals of BfrC protein were obtained by equilibration of 1.5 μ L of 10 mg/mL protein (in 20 mM Tris/HCl, pH 7.5) with 1.5 μ L of reservoir solution (condition G2 or 2-26 from JCSG plus screen; Molecular Dimensions Limited, Calibre Scientific, Rotherham, UK) over an 80- μ L reservoir. Crystallization solution contained 0.02 M of magnesium chloride hexahydrate, 0.1 M HEPES, pH 7.5, and 22% w/v Poly (acrylic acid sodium salt) 5100. Crystals grew within 1 week. Crystals were flash frozen in liquid nitrogen using reservoir solution with 20% glycerol for BfrB and 20% ethylene glycol for BfrC and stored in liquid nitrogen before the data collection.

X-ray data were collected at Diamond Light Source UK, beamline I24 at 100 K using a Pilatus3 6 M detector and 0.999 Å wavelength. Data were integrated during

data collection by Xia2_Dials software⁸⁹ and scaled using AIMLESS⁹⁰ as implemented in the CCP4i2 interface⁹¹ to 1.77 Å for BfrB and 1.8 Å for BfrC. Both crystal structures were solved by MOLREP,⁹² for BfrB using chain A of the holo-HmuY structure (PDB ID: 3H8T) and for BfrC using the model predicted by RosettaCommons server (<https://www.rosettacommons.org/software/servers>). Both models were automatically built by ArpWarp,⁹³ followed by manual model building and restrained refinement using Coot⁹⁴ and REFMAC5.⁹⁵ TLS refinement was used for BfrB. X-ray data collection and refinement statistics are given in Table 1.

2.12 | Molecular dynamics (MD) simulations

MD simulations were performed with Gromacs 2022.4⁹⁶ using the Gromos54A7 force field.⁹⁷ Subunit B of the BrfA crystal structure (PDB ID: 4GBS) was selected for the simulations, replacing methyl-lysine residues with lysine. Models with Fe-heme added manually as covalent links to Met146 or Met175 were constructed. The structures were prepared for MD runs in each case by adding hydrogen atoms and assigning charges to protein residues. Following solvation with SPC water⁹⁸ and charge neutralization with Cl⁻ ions, the simulation box contained ~19 000 atoms. Following energy minimization employing protein restraints, the system was equilibrated under the microcanonical ensemble at a temperature of 310 K for 200 ps and then switched to the isothermal-isobaric ensemble using the Parrinello-Rahman barostat⁹⁹ at 1 atm pressure. The system was further equilibrated for 200 ps. Production runs using a time-step of 2 fs, with replicates for each model, were then made for up to 100 ns. The Particle-Mesh-Ewald (PME) sum method¹⁰⁰ was used for all electrostatic calculations with a cutoff distance of 1.0 nm. MD trajectories were examined using the VMD program.¹⁰¹

2.13 | Bioinformatics and statistical analyses

Comparison of amino acid sequences was performed using the Multiple Sequence Alignment Clustal Omega available from the European Bioinformatics Institute (EMBL-EBI).¹⁰² Three-dimensional protein structures were visualized using the UCSF ChimeraX available from the UCSF Resource for Biocomputing, Visualization, and Informatics (<http://rbvi.ucsf.edu>).¹⁰³ Three-dimensional protein structures of TonB-dependent outer membrane receptors have been modeled using AlphaFold^{104,105} and presented with Swiss-PdbViewer 4.1.0.¹⁰⁶ The statistical

TABLE 1 X-ray data collection and refinement statistics.

Protein (PDB ID)	BfrC (8B61)	BfrB (8B6A)
<i>Data collection</i>		
Space group	P22121	I21
Cell dimensions a, b, c (Å)	52.08, 89.84, 99.06	92.47, 42.31, 110.39
α, β, γ (°)	90, 90, 90	90, 95.49, 90
Resolution (last shell) (Å)	66.8–1.81 (1.84–1.81)	38.44–1.77 (1.81–1.77)
No. reflections (last shell)	43 116(2286)	40 527 (1756)
R_{merge}	0.163(1.421)	0.76 (1.46)
R_{pim}	0.071(0.871)	0.11(1.078)
CC(1/2)	0.996(0.372)	0.983 (0.346)
I/ σ I	6.1(0.7)	4.2 (0.5)
Completeness (%)	99.4(91.6)	96.9 (75.4)
Redundancy	6.0(3.9)	3.9 (2.5)
Wilson B (Å ²)	22.8	13.0
<i>Refinement</i>		
Resolution (Å)	66.8–1.81	38.44–1.77
No. reflections	40 765	38 371
Rwork/Rfree ^b	0.198/ 0.249	0.206/0.259
No. atoms		
Protein	3779	2689
Water	496	523
<i>B-factors (Å²)</i>		
Protein	19.523	19.65
Ligand	23.108	43.36
Waters	39.975	29.83
<i>Rms deviations</i>		
Bond lengths (Å)	0.012	0.013
Bond angles (°)	1.732	1.660

analysis was performed using Student's *t*-test and the GraphPad software (GraphPad Prism 8.0 Inc., San Diego, CA, USA).

3 | RESULTS

3.1 | Compared to *P. gingivalis*, *B. fragilis* encodes three potential HmuY homologs

B. fragilis encodes three potential HmuY homologs, termed here BfrA (*B. fragilis* NCTC 9343 locus ID: BF2707, BF9343_RS12925, BF9343_2622), BfrB (locus ID: BF1028, BF9343_RS04845, BF9343_0985), and BfrC (Locus ID: BF2165, BF9343_RS10160, BF9343_2078) (Figure 1). Comparison of amino acid sequences of proteins belonging to the HmuY family showed differences between them (Figure 2), whereas no differences have been found among proteins produced by examined *B. fragilis* NCTC 9343 and 638R strains (data not shown).

Compared to *P. gingivalis hmu* operon, a slightly different arrangement of genes composing *hmu*-like gene clusters exists in *Bacteroides* species (Figure 1). In *B. fragilis*, similar to *B. vulgatus* and *B. thetaiotaomicron*, upstream of *bfrA* (the gene encoding the first HmuY homolog, BfrA), a gene encoding calycin-like domain-containing protein is located. In the case of the second and third *B. fragilis* HmuY homologs, BfrB and BfrC, shorter operons are composed of genes encoding TonB-dependent outer membrane receptors (HmuR homologs), and PepSY domain-containing protein or DUF4903 domain-containing protein, respectively.

Similar to the first TonB-dependent outer membrane receptor encoded in the *hmu*-like operon of *T. forsythia* (I) and the receptor in the *hmu*-like operon in *P. intermedia*, the receptor encoded close to the *bfrA* gene in *B. fragilis* also possesses two conserved methionine residues, which is in contrast to *P. gingivalis* HmuR^{107,108} and the second outer membrane receptor encoded in the *hmu*-like operon in *T. forsythia* (II), the latter two proteins possessing two

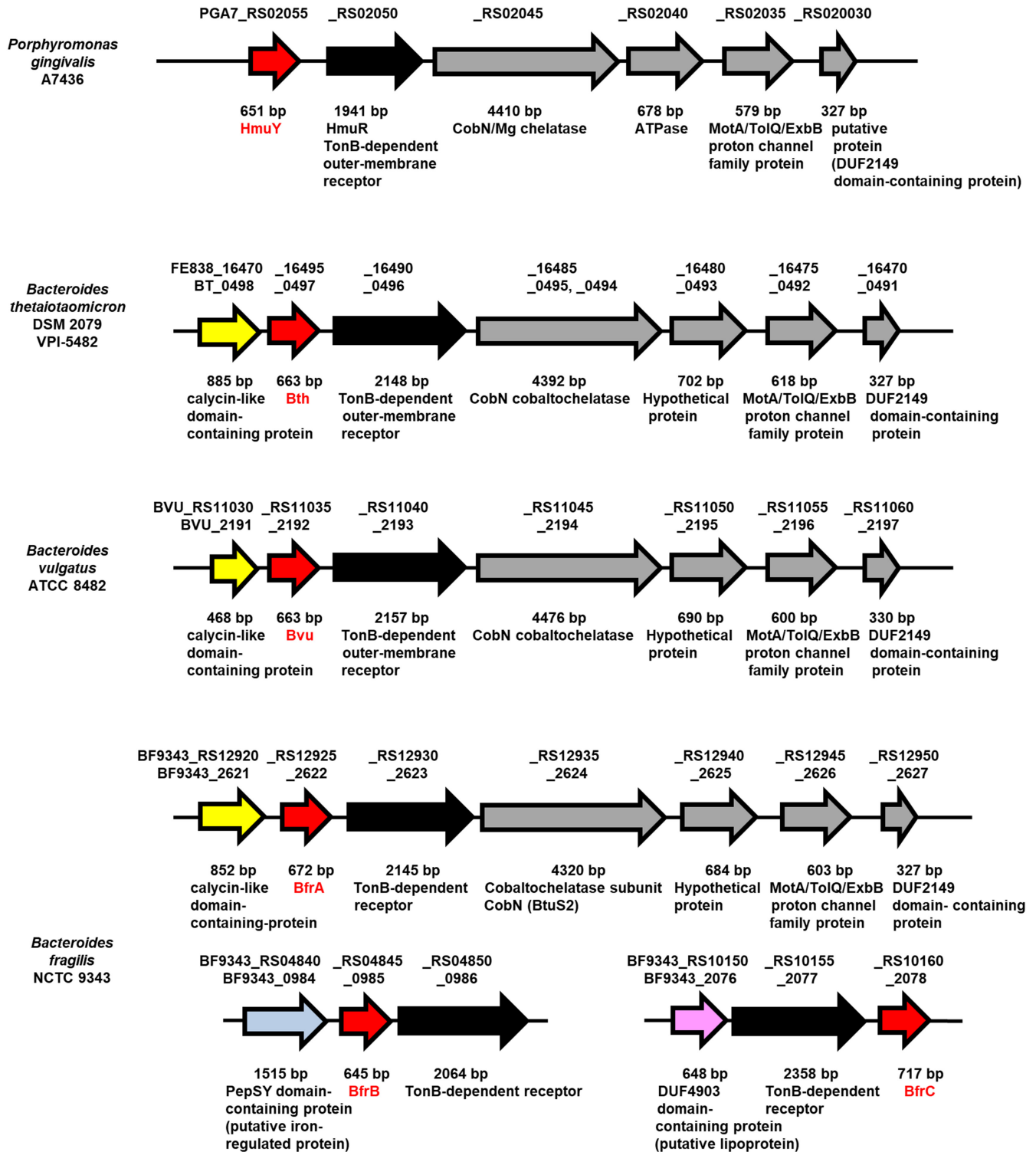


FIGURE 1 Organization of genes encoding *P. gingivalis* HmuY and its homologs in selected *Bacteroides* species. Genes encoding HmuY family proteins are shown in red, genes encoding TonB-dependent outer membrane receptors in black, and additional genes, not present in the *P. gingivalis* *hmu* operon, in yellow, blue, or pink.

conserved histidine residues (Figures S1 and S2). TonB-dependent outer membrane receptors encoded by the genes located close to the *bfrB* and *bfrC* genes do not possess the first conserved methionine or histidine residue

located in a similar position in the conserved plug domain region. Instead, histidine residues are located a few amino acid positions downstream (Figures S1 and S2). In the region located in the β -barrel structure, the receptors

Pg_HmuY	-----MKKIIFSAALCALP-LIVSLTSCGKK-KDE-----PNQPSTPEAV-----	37
Tf_Tfo	-----MKMRNVMTLALV-A-LSLAFVCGDKKDDVKETIKK-----	33
Pi_PinO	-----MKTKIFAVACL---ATLLFTSCSKDNDDPNPKPETTQVK-----	37
Bv_Bvu	-----M-----KRYLSIITILGMLLPFSACDGLILEGI-----YDSPAASDSNELGFIRT	45
Bf_BfrA	MRKA-----ILFCLAITLLGTMLISFSACNGILSSL-----YDEPET---AKDFGFITI	46
Bt_Bth	MRRS-----SNAIFKNIMILG-AAMSLSACNGMFEGI-----YDDPIEAME-----	41
Pi_PinA	-----MKFKSFMALSCL---TVLLFSSCSNDD---PTPKKPEQPKDVPKTLTSLFI--	45
Bf_BfrB	MNNKNKFRFAILLFGVLSAF-----IITACSDN--NS-----PDDPSQGENT-----	40
Bf_BfrC	-----MKHTGLFKTLCFCA-GCLLLSACVDY--SDI-----QPPDGKTL-----	36
Pg_HmuY	-TK---TVTIDASKYETWQYFVSFSKGEVNV-----	64
Tf_Tfo	-----SKTIDATKYEMWTYVNLLETGQETHRDFSE--WHVM-----KNGKLE	74
Pi_PinO	-----HFETLMPGYDSWIYIDLETGKFEQQAELGKREFRKYKSMMDP-----NYEVVG	85
Bv_Bvu	DPSTHSGTIYIDATDYRRWTFIDFHTQKVDVSNVT-----	80
Bf_BfrA	DHANHSGTVRVDATQYTKWNYINLHTLQIDSAKVT-----	81
Bt_Bth	--IKESSFSQINATEYTNWVYIDLSEKATVEIG-----	74
Pi_PinA	-----TQEKAFQGYDKWVYVNLLETGETVMKDDVSEQEWRTYS DAGKKDLFGKYDV--	96
Bf_BfrB	-LPVKQVLSRRTAYGNDWIYYSLEKGEVSV-----	71
Bf_BfrC	-PR---KSGYTTGVNDWIYFNLRTEIFNALGVN-----	67
Pg_HmuY	----TDY--KNDLNWDMLHRYDVRLNCGESGKGGGAVFSGKTEMDQATVPTDGY---	115
Tf_Tfo	TIPAKGSEADIKIKWHIAIHRFDIRTNEGEAIA-----TKETEFSKVTGLPAGD-YKK	126
Pi_PinO	TEPAKGTADLPPKWDIAFHITDARTNNGEVLN-----TGETDLNKINALPAGN-YVA	137
Bv_Bvu	----DSE-QKEPEEWDIAVHRYDVKTNAGAVLE---TGFTGFSALRNADAMPE-GAYVE	130
Bf_BfrA	----AEG-ADDPDWDLAIHRYDVKTNGGEVLE---TDYQSLSALKNAGSMPQ-GIFVA	131
Bt_Bth	----EEHKSEIPAKWDLAIHRYDIKTNEGAFAQ---TTYTSIDDLKASGKLPAAENFVK	126
Pi_PinA	TKTVEGKPSNAPDKWHLAFVFDVRTNGAEACM-----TDTTDIETIKTLPNTVVKVVS	149
Bf_BfrB	----SEESHAENTDWDIAFNRYNVRTNSGASGKGGALLTNIKDLAACTVPPQGT---	124
Bf_BfrC	-RDIKEGGQMNRTDWDLAFCGYVMRTNSGTSIGRGGAADLGYGNENWTSVAQLPSDLK	126
Pg_HmuY	TVDVLGR--ITVK-----YEMGP-----DGHQMEYEEQGFSEVITGKKNA	153
Tf_Tfo	DVEIKDKMLVGFENMA-----DMKSKFTVAGMA---KVPVFLK-----	161
Pi_PinO	DAP---ADIVVDMS-----RMQS-EG-VLGMVKTMLNGEMG-----	168
Bv_Bvu	DVWTTAK--IAIDMS-----GMD--GNIVYMESSYNEELS-----	162
Bf_BfrA	DEWTTNK--IAVDVS-----HMME-DNGYLIYAPSDFNPELS-----	165
Bt_Bth	DEWTTDK--IAIDMS-----GMME--GNIKYTEDYRNDILS-----	158
Pi_PinA	DIK---AYLIYDMT-----GMMKNPV-VMGYMKS YVNMGLY-----	181
Bf_BfrB	TVDAAYT--ITAP-----GTGFP-----P-PTME---STANEVLC-----	153
Bf_BfrC	WVEDNQE--VYVTMSQNDWNHYLIENGLDFNSNPWFD--PNNGPQKTTNANPFLA-----	178
Pg_HmuY	QGFASGGWLEFSH-----GPAGPTYKLSKRVFVRGADGN-IAKVQFTDYQDAELKKG	205
Tf_Tfo	-----TWIVE-----NPMGKAPVLSKSVFVVKFKDGS-YAKIKFTDATNDKQEKG	205
Pi_PinO	-----KWKVS-----NGMGKPKTVMGNVFAVFKNGN-AALIKFKDNLDKTGKKK	212
Bv_Bvu	-----KWLNVDK-----SNMPPTYTSLNKVYMKLKDGT-YAAVRLTNYMNASGVKG	208
Bf_BfrA	-----KWLNVDT-----SEMPPIYTPSNKVYLLRMKDDT-MAAIRLVS YMNAAGIKG	211
Bt_Bth	-----GWLNVDT-----SSMPPIYTMNQVYLIQLKDNNT-YAAIRFTNYTNARGIKG	204
Pi_PinA	-----YWMHKVKGTMGEYALTMSKSDPKKAPVFLVKFKDGS-YAVIQFTGLKDATGKKK	234
Bf_BfrB	-----KAITF-----AGPPPTYTPSDYVFIVRTASGK-YAKLKAKSFYDDEGKSG	197
Bf_BfrC	-----QAMSF-----AGPPPVYTPSYHTYVVRTADGKH YFKIQIISWYDANVEIG	223
Pg_HmuY	VITFTYTYPVK-----	216
Tf_Tfo	HVSFN YEFQPK-----	216
Pi_PinO	AVSFDYKFIKKAK----	225
Bv_Bvu	FMTIDYIYPFEL----	220
Bf_BfrA	YMTFDYIYPYEP----	223
Bt_Bth	YIDFDFLYPLDFEENN-	220
Pi_PinA	EVSFKYKFKVKN-----	246
Bf_BfrB	IYSFEYAIQPDGSTNLN	214
Bf_BfrC	DEGGRLSYYCDELQP--	238

FIGURE 2 Amino acid sequence comparison of *B. fragilis* Bfr proteins with the best-characterized HmuY family members. Amino acids engaged in HmuY in heme binding, experimentally confirmed by site-directed mutagenesis and crystallographic analysis, are shown in red, whilst those confirmed experimentally by site-directed mutagenesis or predicted amino acids engaged in heme binding in HmuY homologs are shown in blue or green, respectively. Pg, *P. gingivalis*; Tf, *T. forsythia*; Pi, *P. intermedia*; Bv, *B. vulgatus*; Bf, *B. fragilis*; Bt, *B. thetaiotaomicron*.

encoded close to the *bfrB* and *bfrC* genes possess conserved histidine residues surrounded by two conserved amino acid motifs (Figures S1 and S2). All these findings suggest a potential heme-binding function of Bfr proteins and subsequent heme transfer through the outer membrane performed by respective TonB-dependent outer membrane receptors. Therefore, we assumed that Bfr proteins may belong to the HmuY family of proteins with hemophore-like properties.

3.2 | Iron/heme levels influence expression of *bfr* genes

We found that, analogously to members of the HmuY family so far characterized, the expression of *bfrA*, *bfrB*, and *bfrC* genes increased when *B. fragilis*, first grown in rich iron/heme conditions (BHIS), was further cultured in conditions of lower iron and heme availability (Figure 3A, open bars). In general, this effect correlated significantly

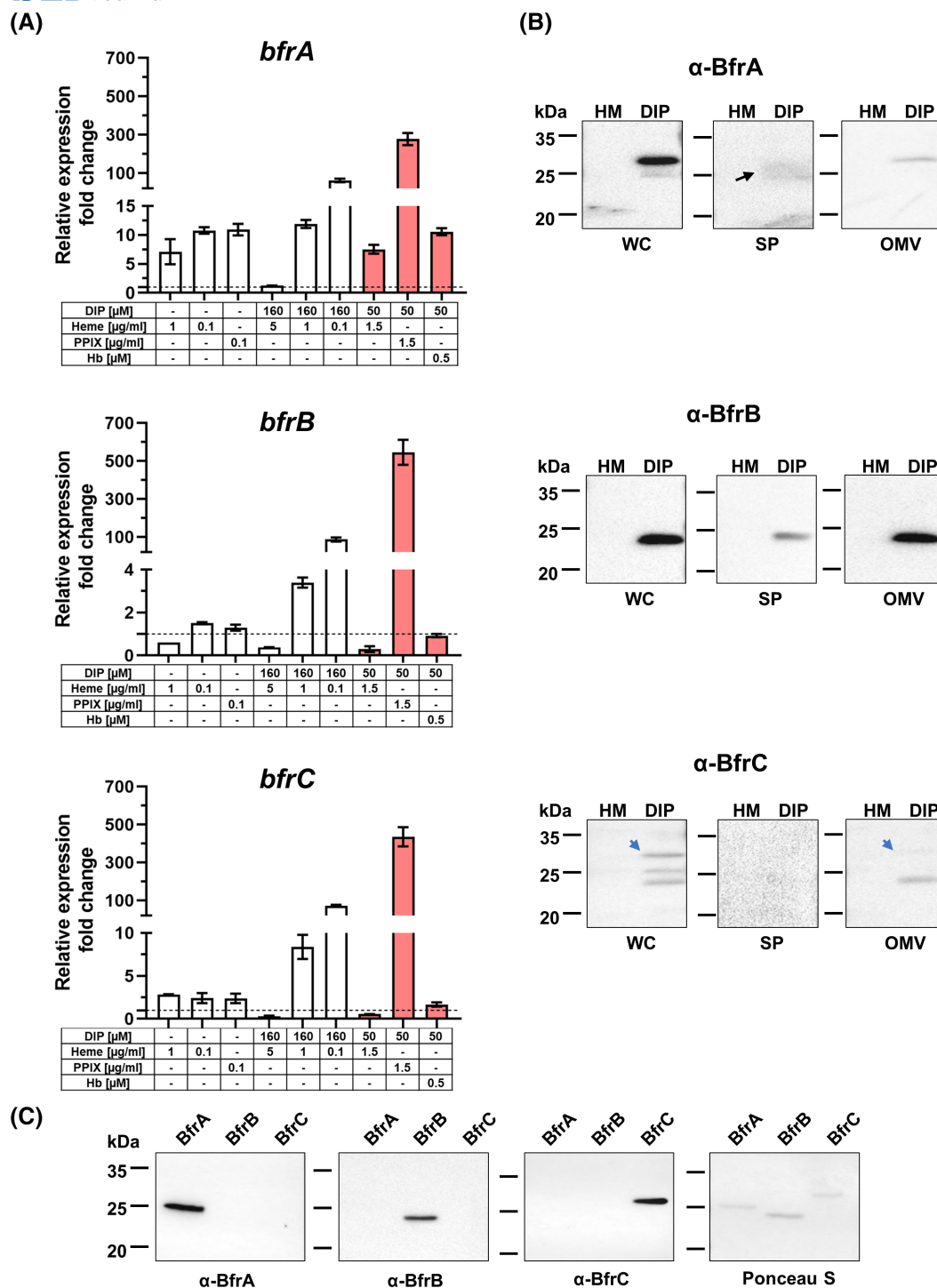


FIGURE 3 Analysis of *bfr* transcripts (A) and Bfr proteins (B) in *B. fragilis* cultured in different conditions. (A) Levels of transcripts analyzed by RT-qPCR. Relative expression fold change represents mRNA levels in bacteria grown in indicated conditions versus bacteria grown in rich iron/heme conditions (BHIS), the latter set as 1.0. Bacteria were cultured in BHIS and then either inoculated into BHIS (reference samples) or into minimal medium (DM) supplemented with indicated compounds and cultured for 24 h (empty bars) or bacteria had been starved of iron and heme (DM without added heme and supplemented with 160 μ M dipyridyl, [DIP]) for 24 h and then inoculated into DM supplemented with indicated compounds and cultured for 24 h (red bars). (B) Levels of proteins analyzed by Western blotting using antibodies directed to respective Bfr proteins (α -BfrA, α -BfrB, α -BfrC). WC, whole bacterial cells; SP, fraction comprising soluble proteins; OMV, outer membrane vesicles; HM, bacteria grown in rich iron/heme conditions (BHIS); DIP, bacteria grown in low-iron/heme conditions (DM without added heme and supplemented with 160 μ M dipyridyl). Black arrow indicates soluble BfrA protein and blue arrows indicate membrane-associated BfrC protein. (C) Specificity of antibodies was analyzed using 250 ng of purified BfrA, BfrB, and BfrC proteins. Ponceau S, proteins stained on a nitrocellulose membrane with Ponceau S.

with decreasing concentration of added heme (from 5 to 0.1 $\mu\text{g}/\text{mL}$) in the presence of 160 μM iron chelator (DIP). The most pronounced increase in respective transcript levels was observed in the case of bacteria grown in DM medium supplemented with 160 μM DIP (ensuring iron chelation) and 0.1 $\mu\text{g}/\text{mL}$ heme (ensuring bacterial proliferation): fold change increase ~ 60 , ~ 90 , and ~ 70 for *bfrA*, *bfrB*, and *bfrC*, respectively. Only *bfrA* gene expression was higher when bacteria had been cultured in the presence of iron (derived from DM medium) and with a very low concentration of heme (1.0 or 0.1 $\mu\text{g}/\text{mL}$) or PPIX (0.1 $\mu\text{g}/\text{mL}$). In addition, we examined gene expression in bacteria further starved of iron and heme. For this purpose, we first grew bacteria in minimal medium (DM) without added heme or PPIX, but supplemented with 160 μM DIP, and then in DM supplemented with 50 μM DIP and heme, PPIX, or hemoglobin (Figure 3A, red bars). Expression of all genes increased when DM was supplemented with PPIX in the presence of DIP, suggesting an insufficient amount of iron to form heme from available iron and PPIX amounts. Only mRNA encoding the BfrA protein increased when free heme or heme bound to methemoglobin was used as a heme source with limited access to iron (50 μM DIP). Similar to transcript levels, all Bfr proteins were also produced at higher levels when bacteria had been starved of iron and heme (Figure 3B).

Fractionation of *B. fragilis* cultures showed that the BfrA protein was associated mainly with the whole bacterial cell, with a small amount present in the fraction comprising outer membrane vesicles (OMV), as well as in the form of soluble protein (Figure 3B). The distribution of BfrB protein in all fractions examined was similar to that observed for *P. gingivalis* HmuY, whereas the BfrC protein was found mainly in the form associated with the whole bacterial cell and with OMV. Among all examined antibodies which were directed against Bfr proteins, anti-BfrC antibodies exhibited the lowest specificity and sensitivity (Figure 3B,C).

3.3 | Bfr proteins differ in their stability as compared to *P. gingivalis* HmuY protein

All Bfr proteins are less resistant to thermal denaturation than HmuY and its homologs so far characterized (Figure S3).^{73,74} Among all the proteins examined in this study, similar to *P. intermedia* PinO, only BfrB was able to refold after thermal denaturation. The addition of heme to Bfr proteins did not significantly influence their susceptibility to thermal denaturation. Compared to HmuY, all Bfr proteins were degraded in *P. gingivalis* cultures (Figure S4). However, neither HmuY nor Bfr proteins were degraded when added to *B. fragilis* cultures.

3.4 | BfrA and BfrB may bind heme but in a manner different from *P. gingivalis* HmuY

Heme-binding ability was first examined using concentrated purified, recombinant proteins, possessing the N-terminal 6 \times His and maltose-binding protein (His-MBP fusion tag) which had been overexpressed in *E. coli*. UV-visible absorption spectral maxima were observed only in the case of BfrA and BfrB, suggesting heme binding (Figure S5A). Subsequently, samples of proteins lacking the fusion tag and complexed with heme were examined visually (Figure S5B), which revealed a color typical for heme-binding proteins in the case of BfrA and BfrB. Based on these preliminary findings, we assumed that BfrA and BfrB may bind heme.

Free ferric heme in solution exists as a monomer-dimer equilibrium, giving absorption maxima in the Soret region at 365 and 385 nm (Figure 4). In the BfrA-Fe(III)heme complex, in addition to the broad Soret peak at ~ 401 nm, a broad, low-intensity feature in the Q band region at ~ 529 nm could also be observed (Figure 4A). Upon reduction with sodium dithionite, a single Soret maximum is seen at 426 nm, with well-resolved asymmetric bands in the Q band region at 528 and 558 nm (Figure 4B). After re-oxidation, the ferrous form shifts back to the ferric form (Figure 4C). In the BfrB-Fe(III)heme complex, the Soret peak has a maximum at 391 nm (Figure 4A), the Q bands are found at 512 and 544 nm, and the charge transfer CT1 band is located at 645 nm. Interestingly, upon reduction, multiple maxima could be observed in the Soret region at 414, 433, and 446 nm (Figure 4B), and Q band maxima are clearly visible at 538 and 571 nm. After re-oxidation, the ferrous form shifts back to the ferric form with a maximum of 398 nm (Figure 4C). Heme-binding features of BfrA and BfrB proteins were further confirmed by measuring UV-visible absorption difference spectra (Figure S6).

Although BfrA and BfrB bind heme, differences in binding strength can be observed. The strongest heme binding was found for BfrA under reducing conditions ($K_d = 6.42 \pm 0.83 \times 10^{-8}$ M) and for BfrB under air (oxidizing) conditions ($K_d = 1.4 \pm 0.3 \times 10^{-8}$ M). The heme bound to BfrA was mostly lost during size-exclusion chromatography under air (oxidizing) conditions, whereas in the case of BfrB, a small portion eluted in complex with heme (Figure S8). Under reducing conditions, only BfrA was able to preserve bound heme. As shown in Figure (Figure S7), only BfrA may bind modified hemes, FeDPIX and FeMPIX, and only under reducing conditions.

Based on the UV-visible absorption spectra, we suspected that BfrA and BfrB proteins may have evolved specificity not only toward heme binding through heme iron coordination, but could also bind iron-free PPIX.

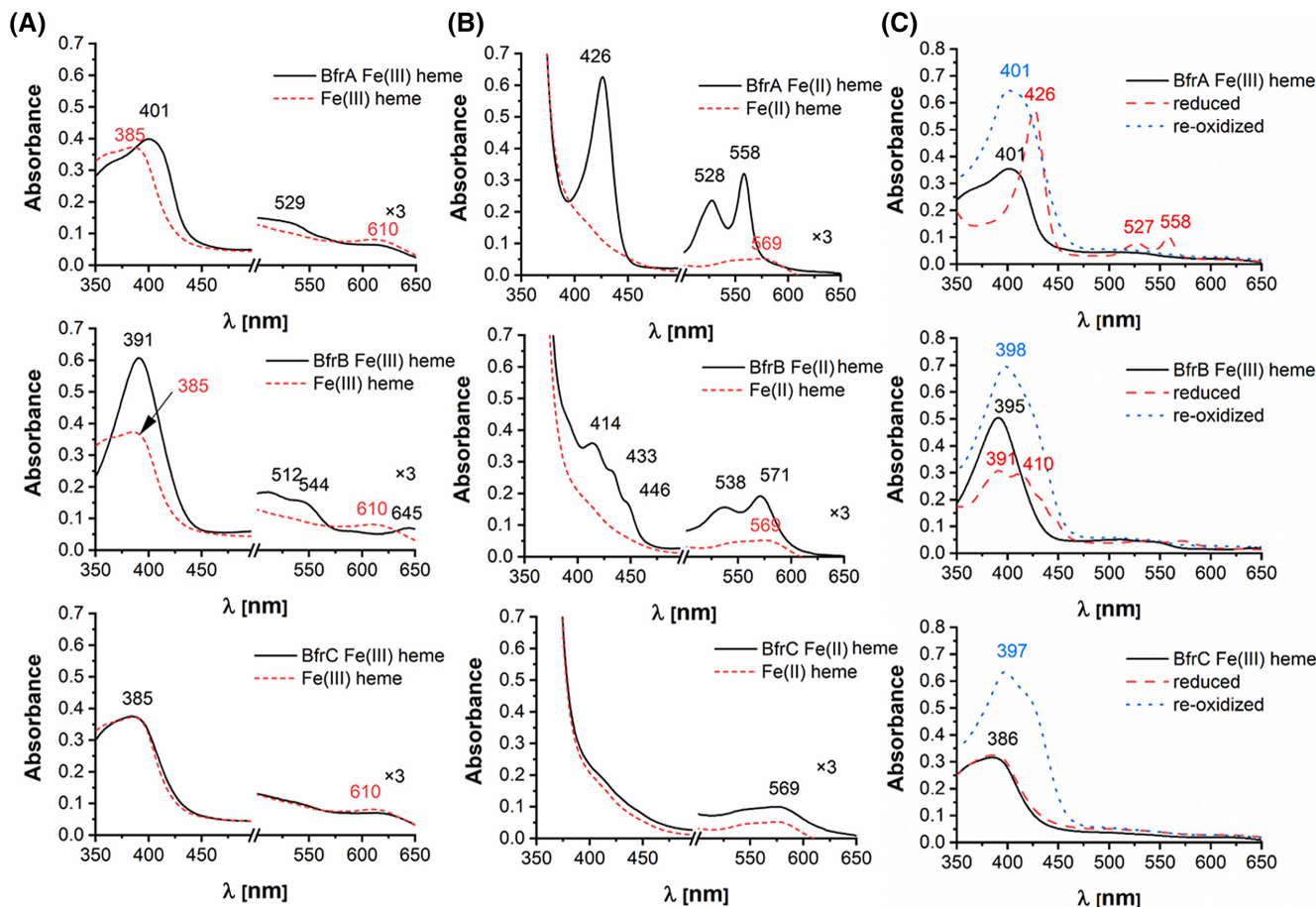


FIGURE 4 Analysis of heme binding to purified Bfr proteins. Proteins (5 μ M) were titrated with heme under air (oxidizing) (A) or reducing (B) conditions. Proteins in complex with heme were also monitored under air (oxidizing conditions), subsequently reduced by sodium dithionite, and re-oxidized by potassium ferricyanide (C). Protein-heme complex formation was monitored by UV-visible absorbance spectroscopy.

Among all the Bfr proteins tested, only BfrB was able to efficiently form a complex with PPIX under air (oxidizing) conditions ($K_d = 9.8 \pm 2.89 \times 10^{-8}$ M) (Figure 5A, left panel, Figure 5B,C), and with lower ability under reducing conditions ($K_d = 1.6 \pm 0.2 \times 10^{-6}$ M), similar to *P. gingivalis* HusA.⁸²

Similar to *P. gingivalis* HmuY,^{84,85} the binding of PPIX to other Bfr proteins seems to be significantly lower (Figure 5D,E, left panel). We also observed that BfrB is able to bind CPIII, although with lower efficiency as compared to PPIX (Figure 5A, right panel, Figure 5B,C). However, in contrast to heme and PPIX, CPIII did not support *B. fragilis* growth (S9 Figure). For comparison, we examined binding of PPIX and CPIII to *P. gingivalis* HmuY and HusA (Figure 5D,E). HmuY bound CPIII, similar to human serum albumin (HSA), whereas HusA was not able to bind CPIII.

In contrast to BfrA and BfrB, we did not find evidence of an interaction of BfrC with all porphyrins examined under conditions used in this study (Figures 4 and 5 and Figures S5–S8).

3.5 | Three-dimensional structures of BfrB and BfrC proteins are similar to BfrA and HmuY

The three-dimensional structure of *B. fragilis* BfrA (PDB ID: 4GBS) in the apo-form has been determined and deposited in the database by others (the Joint Center for Structural Genomics, JCSG, La Jolla, CA, USA). In this study, we determined three-dimensional structures of *B. fragilis* BfrB and BfrC proteins by X-ray crystallography (Table 1).

The crystal structure of BfrB (PDB ID: 8B6A), determined at 1.77 Å resolution, has two identical chains in the asymmetric unit. Each chain contains a β sandwich in its core, formed by two β sheets; one with four antiparallel β strands and another from five antiparallel β strands composed of non-consecutive residues (Figure 6A and Figure S10A). In total, the structure contains 13 β strands and three small α helices. The positively charged Fe cavity (Figure S10B) is located on the side of the core among three extended loops; two of them contain two antiparallel

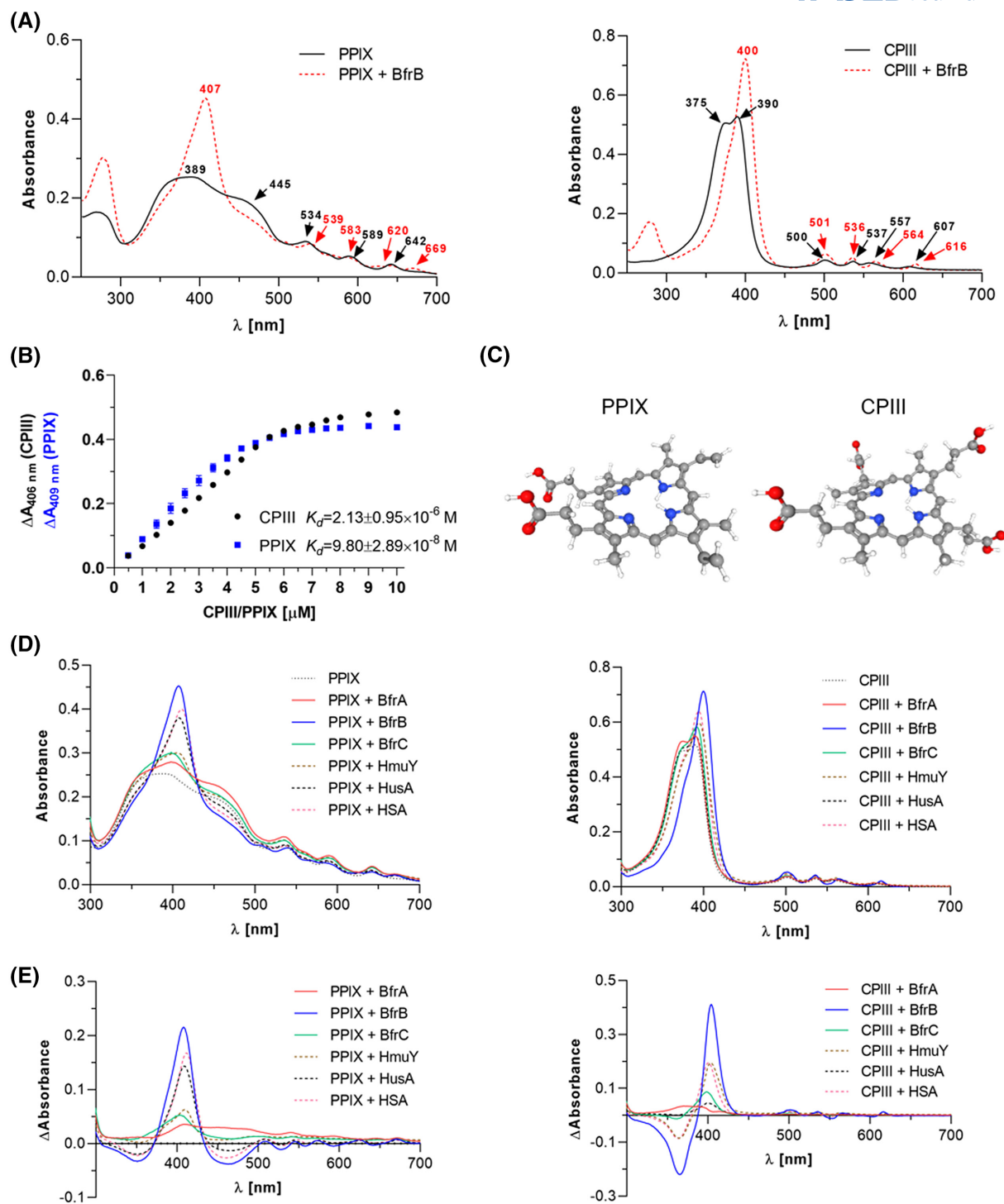


FIGURE 5 Analysis of protoporphyrin IX (PPIX) and coproporphyrin III (CPIII) binding to examined proteins. Proteins (5 μ M) were incubated with an equimolar concentration of PPIX or CPIII (A, D, and E), and the protein-porphyrin complex formed was monitored by UV-visible absorbance spectroscopy (A and D) or difference absorption spectra were recorded (E). Dissociation constants (K_d) of BfrB-PPIX and BfrB-CPIII complexes were determined using titration of 5 μ M BfrB protein with PPIX or CPIII (B). PPIX and CPIII structures were obtained from PubChem (<https://pubchem.ncbi.nlm.nih.gov/>). Atoms in the structures are colored in gray (carbon), white (hydrogen), red (oxygen), and blue (nitrogen). BfrA, BfrB, BfrC, *B. fragilis* HmuY homologs; HmuY, *P. gingivalis* hemophore-like protein; HusA, another *P. gingivalis* hemophore-like protein; HSA, human serum albumin.

β strands and connect by a short α helix. Interestingly, this cavity site does not contain His or Met residues, but among others, it has residues identical to those responsible

for heme binding in HmuY: Tyr54, Tyr165, Tyr89, Arg88, and Thr133 (Figure 6A). A negatively charged sulfate ion (SUL), which comes from the crystallization solution,

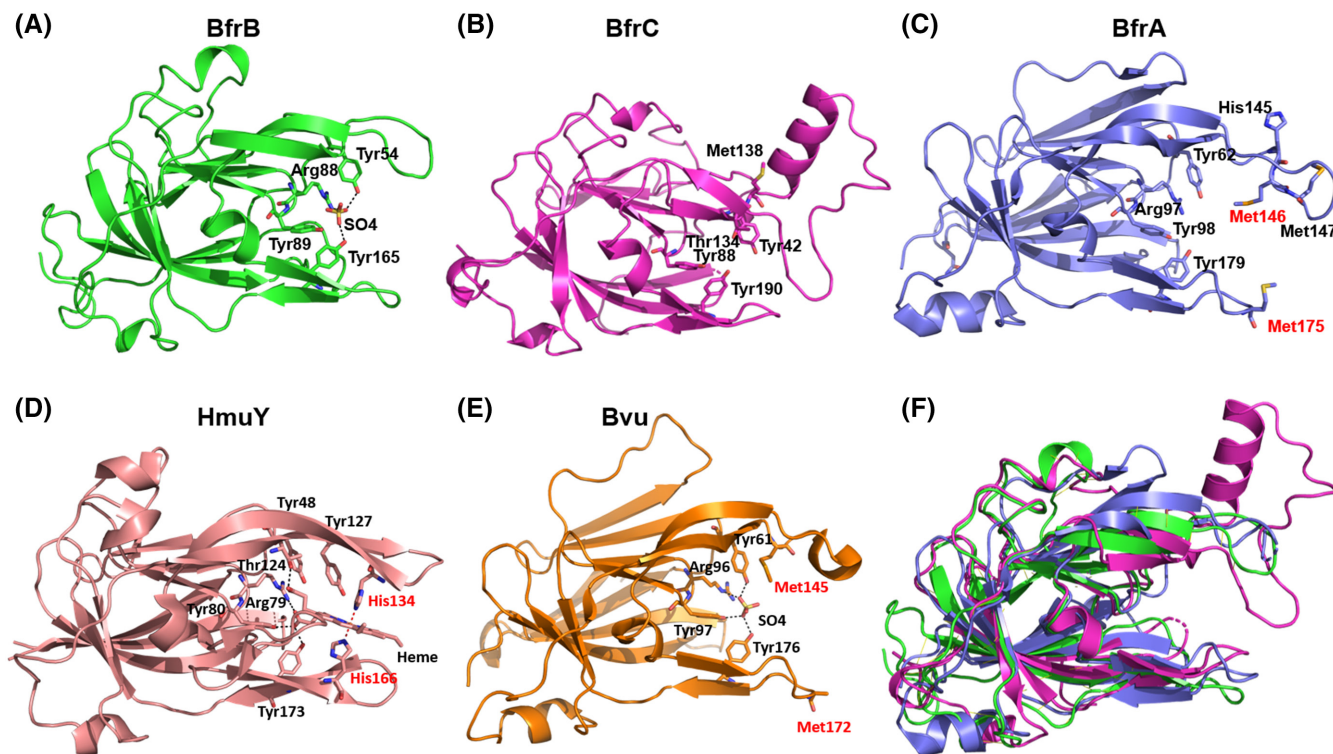


FIGURE 6 Comparison of the overall structures and central cavity features of hemophore-like proteins. Apo-protein structures of *B. fragilis* Bfr proteins (A–C) and *B. vulgatus* Bvu protein (E) are compared with HmuY-heme complex (D). Amino acids potentially involved in heme iron coordination are indicated in red. Overlap of structures of all hemophore-like proteins is shown in (F).

is bound within this site, ligated by Tyr54, Tyr165, and Arg88. It is possible that the sulfate ion is bound by amino acid residues responsible for the heme binding, but not as strongly as heme in HmuY (Figure S10C).

The crystal structure of BfrC (PDB ID: 8B61), determined at 1.81 Å resolution, also has two identical chains in the asymmetric unit. Each chain consists of a roughly globular β sandwich of two β sheets composed of four antiparallel β strands and six antiparallel β strands from non-consecutive residues (Figure 6B and Figure S10A). In total, the BfrC structure consists of 5 β sheets, 6 β hairpins, 5 β bulges, 15 β strands, 6 α helices, 22 β turns, and two γ turns. Two arms are protruding from the main body of the protein, both composed of two β sheets with the longer arm containing a long flexible loop and small helical structure. The top arm extends beyond the others due to the presence of a longer loop and a helix formed by 11 amino acid residues. Poly(acrylic acid), which comes from the crystallization solution, is bound in a cleft of the long arm, which can indicate the possible ligand binding pocket. Interestingly, the only residues from the heme-binding pocket of HmuY are maintained in BfrC, i.e., Thr137 and Tyr88, which could explain the difficulty of heme binding. Based on the structural data, the three-dimensional structure of BfrB (Figure 6A) is similar to BfrA (Figure 6C), HmuY (Figure 6D), and Bvu (Figure 6E).

Structural comparison of HmuY homologs so far characterized shows a similar overall fold of the core (Figure 6F). Rms deviation between 189 Cα atoms of BfrC chain A and Cα atoms of HmuY chain A (PDB ID: 3H8T) is ~2.2 Å and ~2.5 for matching secondary structure; for 181 Cα atoms of BfrB it is 1.45 Å and 0.85 Å for matching 111 Cα atoms; for BfrA it is 1.24 Å for matching 98 Cα atoms. The central cavities positioned similar to the heme-binding pocket of HmuY are positively charged in all four proteins (Figure S10B). The main differences are in the conformation of extended loops surrounding the central cavity (Figure 6), residues located in the heme-binding pocket itself, and in the opening of the cavity. In HmuY, His134 and 166 are responsible for iron heme coordination, while Arg79, Tyr80, Thr124, and Tyr173 are responsible for heme binding (Figure 6D). In BfrB conserved Arg88, Tyr89, Thr133, and Tyr165 are present, which could allow for binding of the heme molecule (Figure 6A). In BfrC many residues taking part in heme binding in other homologous proteins are missing (Figure 6B). BfrA, BfrB, and BfrC have similar β sheet arrangement of the core,⁸¹ but they are different in the extended loop length and conformations and the opening of the central cavity. The structure of BfrB is closer to BfrA; alignment for 89 core Cα atoms of BfrB to BfrA gives 1.45 Å rms deviation, while for 93 Cα atoms of BfrC aligned to BfrA, rms deviation

is three times bigger at 4.53 Å, which is due to the wider opening of the BfrA heme-binding cavity (Figure 6F).

3.6 | BfrA coordinates heme iron

Our attempts to crystallize HmuY homologs in complex with heme or PPIX failed. Therefore, to identify potential heme iron coordinating ligands, we singly replaced several amino acid residues (indicated by amino acid sequence comparisons, crystallographic data, and theoretical modeling) with an alanine residue and analyzed the ability of BfrA site-directed mutagenesis variants to bind heme. UV-visible absorption spectra recorded under oxidizing conditions, where heme is bound to BfrA weakly, demonstrated that single amino acid substitution of all examined potential heme ligands (His145, Met146, Met147, and Met175) resulted in a slight blue shift of the Soret maximum compared to that recorded for the native protein, suggesting a disturbance in heme binding (Figure 7A). Under reducing conditions, a significant effect on heme binding to the M175A variant could be observed (Figure 7B). Determination of heme dissociation constants confirmed weaker heme binding to all BfrA mutagenesis variants under air (oxidizing) conditions (Figure 7A). Under reducing conditions, substitution of Met175 resulted in a significantly decreased ability of heme binding. In addition, a lower binding ability could be observed in the case of the Met146Ala variant (Figure 7B).

No significant changes in the UV-visible spectra were observed for the modified BfrB protein variants as compared to the unmodified BfrB protein, suggesting no heme iron coordination (Figure 7).

Further, MD simulations were performed using a starting BfrA structure (PDB ID: 4GBS) with either Fe(heme)-S(Met175) or Fe(heme)-S(Met146) 'bonds' in place. Simulations with Fe-Met146 exhibited closure of the open loops (from the initial crystal structure) and interaction with Met175 as a possible outcome of the protein dynamics. Figure 8A shows the changing distance between the Fe atom attached to S(Met146) and the S atom (red line) and backbone O atom (black line) of Met175, for two independent MD runs. In the starting model based on the crystal structure, these two methionine residues are about 12 Å apart. The closest approach of S or O of Met175 to the Fe is ~2.8 Å (Figure 8B). As shown in Figure 8A, there is persistent 'contact' between the Met175 and Fe(heme)-Met146 once this configuration is first formed (after ~70 ns in one simulation and ~5 ns in the other). Obviously, no bond between these atoms can be formed in the simulations, but the result indicates the possibility that both methionine residues are capable of binding the heme (given that heme binds to Met146). Similar MD runs were

carried out for an initial setup with Fe(heme) bound to S(Met175), but no identical close interactions with Met146 were found in the current set of simulations.

3.7 | BfrA sequesters heme from host serum albumin

To examine whether HmuY homologs from *B. fragilis* can function as hemophore-like proteins, we analyzed their ability to sequester heme bound to host hemoproteins. UV-visible absorbance analysis demonstrated that only BfrA could sequester heme from the serum albumin-heme complex, and only under reducing conditions (Figure 9A). The ability of heme sequestration from hemopexin by BfrA is possible under reducing conditions, but not convincing due to very similar absorption maxima for both proteins (Figure 9B). None of the Bfr proteins was able to sequester heme bound to hemoglobin, even that bound to the methemoglobin form (Figure S11).

3.8 | HmuY sequesters heme bound to BfrA and BfrB

To analyze any possible competition in heme acquisition between *P. gingivalis* and *B. fragilis*, we examined potential heme transfer between the HmuY and Bfr proteins. We found that HmuY efficiently sequestered heme which had been bound to BfrA (Figure 10A) and BfrB (Figure 10B) under both air (oxidizing) and reducing conditions. In contrast, BfrA and BfrB were not able to capture heme bound to HmuY.

4 | DISCUSSION

To obtain a desired breakthrough in the field of understanding and treatment of infection-based inflammatory diseases, it is first necessary to characterize the proteins crucial to the growth and virulence of key members of the human microbiome, especially those responsible for the cause of dysbiosis. One of the most important growth-stimulating and virulence factors for members of the Bacteroidetes phylum is heme when a non-heme iron source is available.^{44,45,48,62} In vivo, free heme is not readily available because it is toxic and is therefore rapidly bound by host heme-scavenging proteins, which maintain the concentration of the free heme at very low levels.^{110–115} In advanced periodontitis or in intestinal diseases, free heme is released mainly as a result of bleeding and hemolysis, and the subsequent proteolysis of hemoglobin. There is also an intracellular

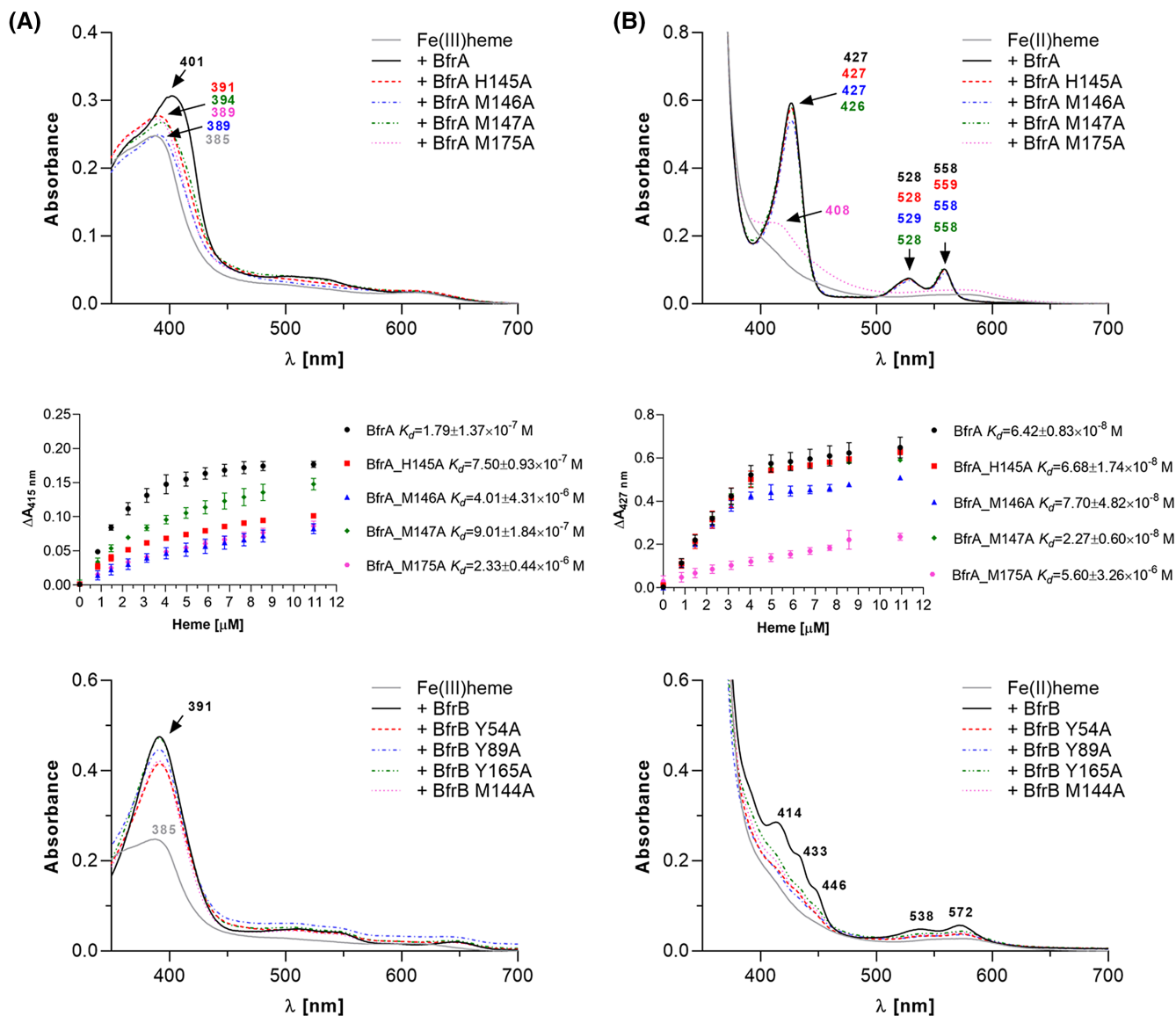


FIGURE 7 Analysis of site-directed mutagenesis variants of BfrA and BfrB proteins in complex with heme. UV-visible absorption spectra were recorded for the protein-Fe(III)heme complexes (A) and protein-Fe(II)heme complexes (B). All spectra were recorded at a 1:1 protein:heme molar ratio for singly replaced selected amino acid residues by an alanine residue in BfrA or BfrB proteins. Dissociation constants (K_d) were determined using difference absorbance spectra measurements during titration of 5 μ M BfrA protein and its variants with heme.

pool of labile heme, present at the highest level in the cytoplasm^{116,117} or that released from cytochromes.¹¹⁸ Importantly, heme present in dietarily consumed hemoglobin and myoglobin forms the largest source of iron and PPIX for gut bacteria.¹¹⁹ It has been demonstrated in a mouse intestinal colonization model that dietary heme can enhance the abundance of Gram-negative *Bacteroides* species relative to the Gram-positive *Firmicutes* population.^{120,121} Moreover, co-infection of *B. fragilis* with a hemoglobin protease producing an *E. coli* strain during experimental polymicrobial infection enhanced the ability of *B. fragilis* to utilize iron from heme.¹²² Also, among human hemoproteins, serum

albumin and hemopexin can serve as important heme sources for pathogenic bacteria, especially those spreading into different niches of the human body, which is the case of both *P. gingivalis* and *B. fragilis*. Although hemopexin can be bacteriostatic for *B. fragilis* for a limited period, the bacterium secretes a protease capable of degrading this hemoprotein, with resultant heme release.¹²³ It is also worth mentioning that bacteria must adapt to oxidative stress due to the presence of heme and iron excess in the gut which otherwise may be toxic. One of the possible ways of mitigating this potential toxic effect could be via expression of hemophore-like proteins to bind and neutralize excess heme.

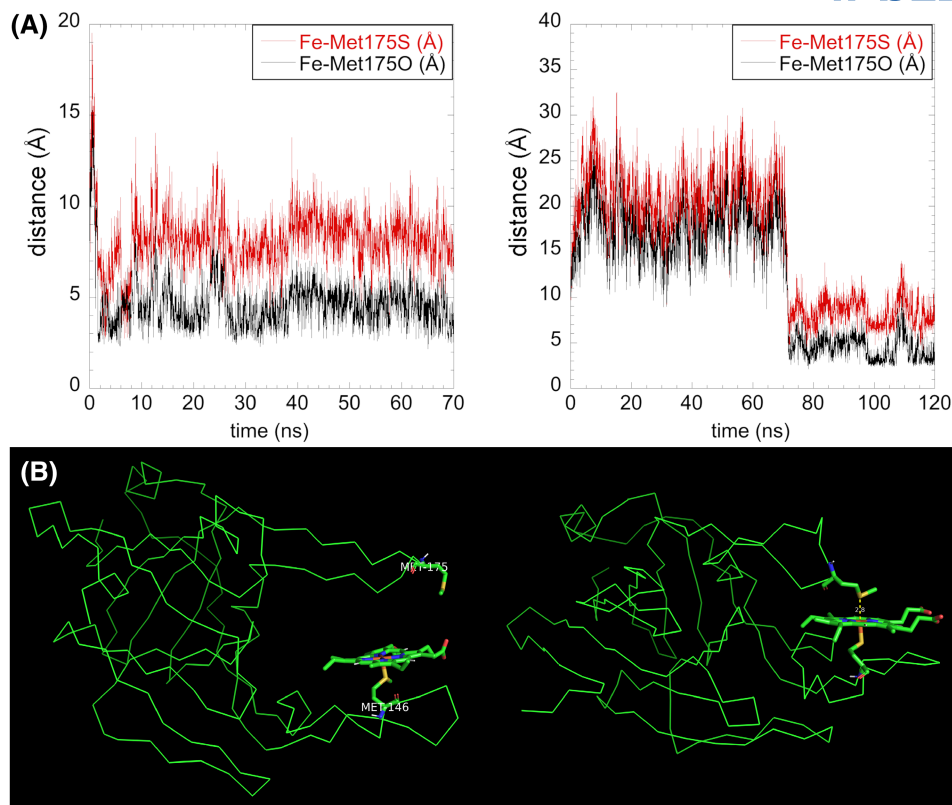


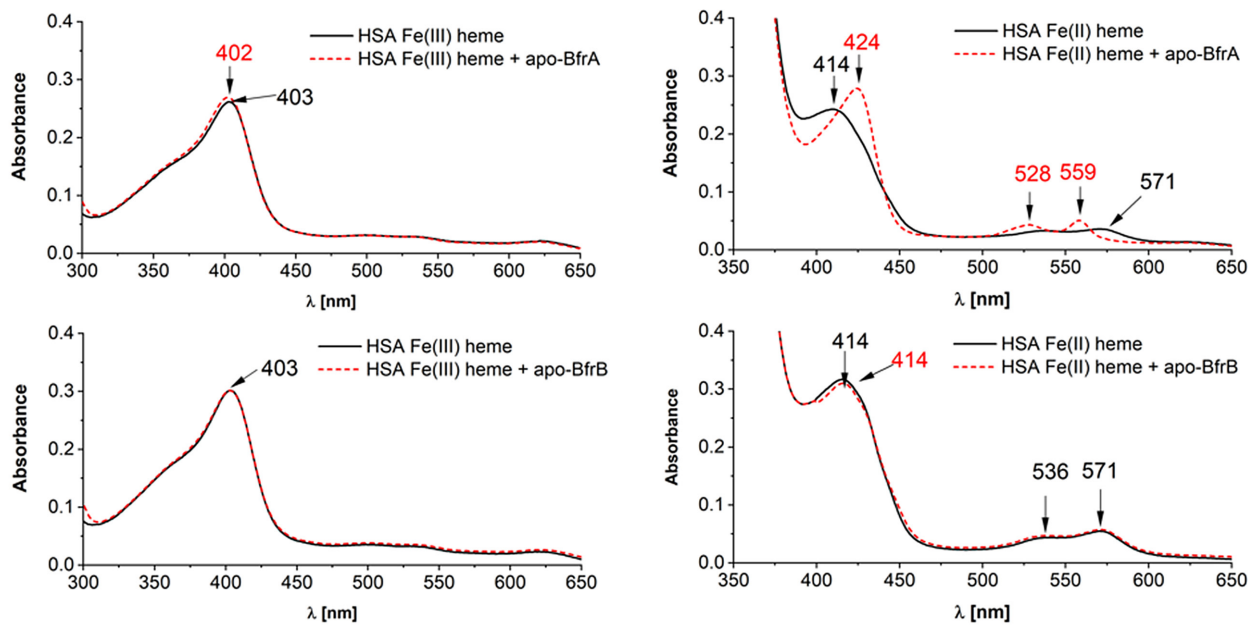
FIGURE 8 Molecular dynamics of Fe(heme)-Met146 models constructed from the BfrA crystal structure. (A) The distances between the Fe atom and the sulfur and backbone oxygen atoms of Met175 from two independent MD simulations are shown. The left panel shows a close and persistent contact between Fe-Met146 and Met175 throughout the simulations. In the right-hand panel, the separation between Fe-Met146 and Met175 fluctuates from ~12 to ~24 Å for the first 70 ns before the structure adopts a configuration with a much shorter separation (~3 Å), which is maintained for the next 50 ns. These close contacts suggest that both Met residues can be considered as potential ligands to the Fe-heme. No other amino acid residues besides Met175 made similar close contacts to Fe-Met146 during the simulations. (B) The left panel shows the Fe(heme)-Met146 construct on the crystal BfrA protein structure. This was the starting structure used for the MD simulations. The right panel shows a snapshot during MD simulations capturing the close contact interaction (2.8 Å) between Fe(heme)-Met146 and Met175.

We hypothesize that *B. fragilis* may utilize related heme acquisition mechanisms, similar to the Hmu system of *P. gingivalis*. The genetic organization of respective genes located in the *P. gingivalis* *hmu* operon, in *hmu*-like operons in other periodontopathogens, and in *hmu*-like gene clusters in other Bacteroidetes members so far characterized^{55,73,74,76} is different from their typical counterpart *hem* operons found in other Gram-negative bacteria.^{124,125} Compared to *E. coli*, members of the Bacteroidetes phylum possess a different outer membrane architecture, rich in lipoproteins and TonB-dependent outer membrane receptors,^{126,127} including Bfr proteins^{128–130} (and this study). Based on the proximity of all *bfr* genes to genes encoding outer membrane transporters, we conclude that Bfr proteins could promote nutrient acquisition, including internalization of heme or iron-free porphyrins. Moreover, the high capacity of *B. fragilis* to generate antigenic variation of surface components,¹³¹ including production of three HmuY homologs, may be useful when *B. fragilis* escapes

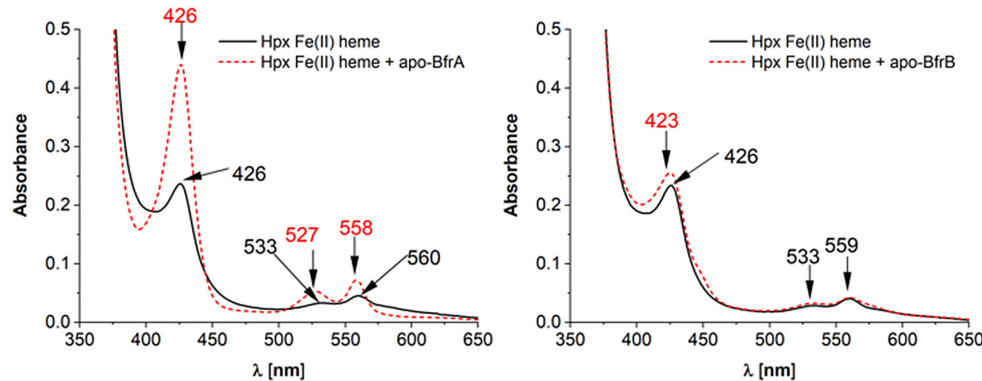
into other body niches, where iron and heme are efficiently sequestered by iron- and heme-scavenging host proteins. The albumin-heme complex can be an important vital heme source for *B. fragilis*, through heme sequestration performed by BfrA. This feature could enhance higher *B. fragilis* potential to generate opportunistic infections, as compared to *B. vulgatus* or *B. thetaiotaomicron*.

Expression of all genes was regulated by iron, and low levels of iron increased gene expression, which could be helpful for *B. fragilis* to produce Bfr proteins in host niches other than the gut. In addition, *bfrA* gene expression was higher when bacteria had been starved of iron and heme and then cultured in the presence of heme or hemoglobin with limited availability of iron. Such conditions ensure cell proliferation but do not provide sufficient amount of heme, which results in higher *bfrA* mRNA production. This suggests potential regulation of the *bfrA* gene expression also by heme and engagement mainly of BfrA in heme supply as an iron and PPIX source. However, it

(A)



(B)



(C)

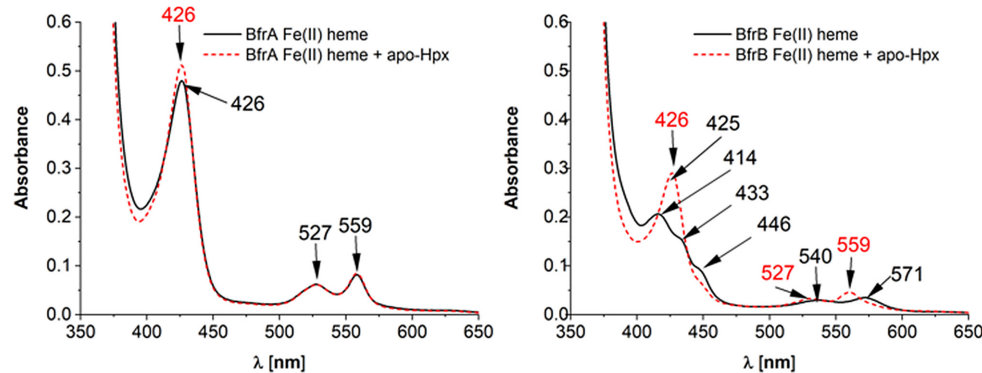


FIGURE 9 Heme transfer between Bfr proteins and host hemoproteins. *B. fragilis* BfrA and BfrB proteins were incubated with an equimolar concentration of (A) human serum albumin (HSA) or (B and C) hemopexin (Hpx) under air (oxidizing) conditions (A, left panel) or reducing conditions formed by addition of sodium dithionite (A, right panel, B, and C). Changes in the spectra were monitored using UV-visible absorbance spectroscopy.

is also worth mentioning that, compared to *bfr* genes, expression of the *hmuY* gene increases up to ~1200 times, depending on the growth conditions, growth phase, and examined strain.^{73,74}

Detailed characterization of the HmuY-heme complex has demonstrated that both Fe(II)PPIX and Fe(III)PPIX are in a low-spin hexa-coordinate environment in the protein, and His134 and His166 are ligands

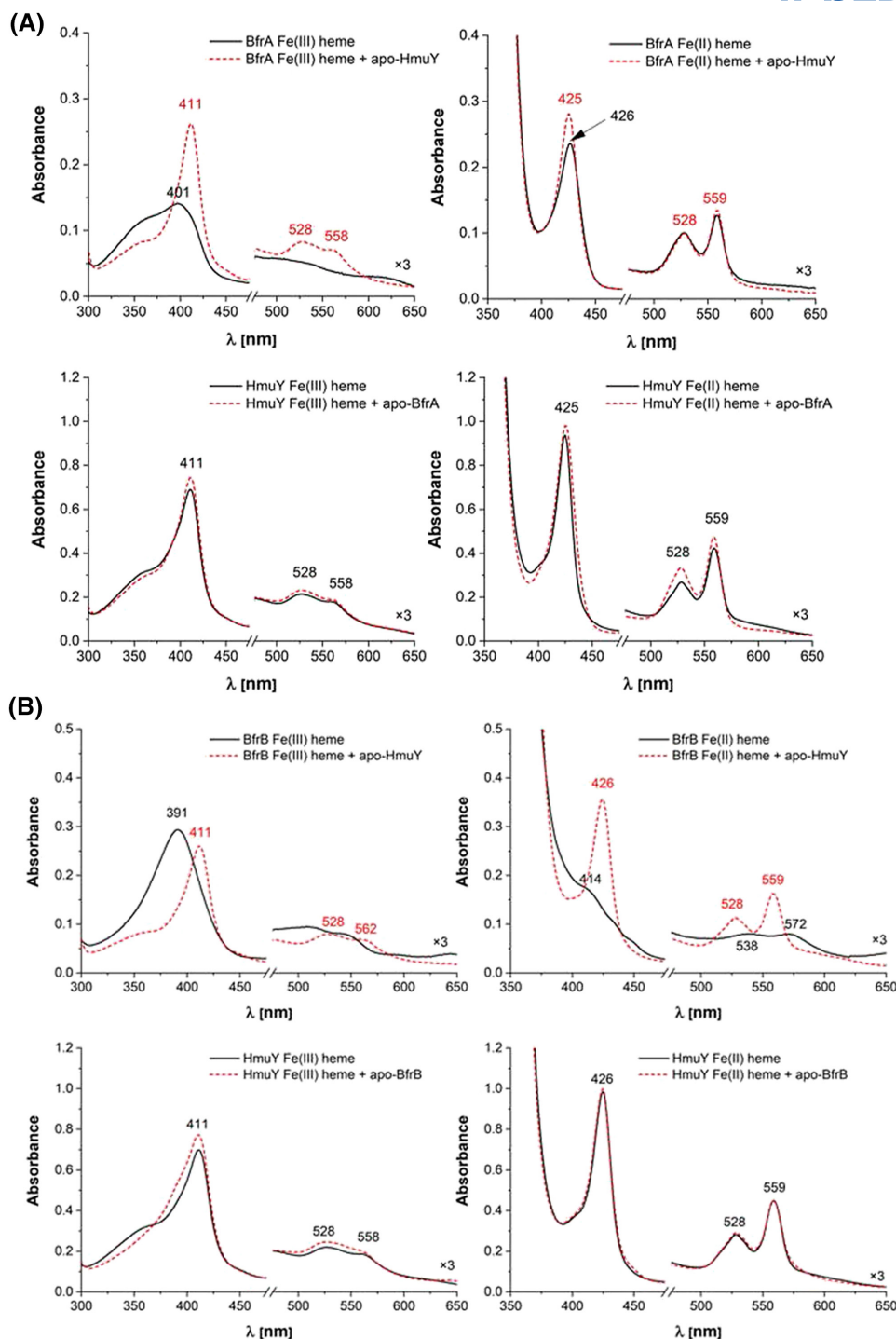


FIGURE 10 Heme transfer between Bfr proteins and HmuY. BfrA (A) or BfrB (B) proteins in apo-form or in complex with heme were incubated with equimolar concentrations of apo-HmuY or with HmuY-heme complex under air (oxidizing) conditions (left panel), or reducing conditions formed by the addition of sodium dithionite (right panel). Changes in the spectra were monitored using UV-visible absorbance spectroscopy.

coordinating the heme iron.^{83,84} In contrast to HmuY, the UV-visible absorption spectra of BfrA in complex with heme are rather characteristic of a pentacoordinate high spin ferric heme bound to the protein, with the sixth coordination position available to other ligands. Under reducing conditions, however, hexacoordinate

low-spin ferrous heme can be observed. We first assumed that BfrA could use Met175 and another methionine (Met146, Met147) or histidine (His145) residue to coordinate the heme iron, preferentially under reducing conditions. Results obtained from MD simulations indicated that Met175 and Met146 could serve

as heme iron coordinating ligands. This process might occur similar to *B. vulgatus* Bvu, where two methionine residues could be engaged in heme iron coordination, preferentially under reducing conditions.⁷⁶ The lack of significant changes in UV-visible absorption spectra of the BfrA-heme complex recorded under reducing conditions for singly substituted protein variants could be due to the supportive engagement of the surrounding amino acid residues (Met147, or less probably His145) in heme binding, similar to the supportive role of Met136 in the HmuY protein after substitution of His134.^{83,132}

The BfrA protein might also be used to deliver modified hemes into the *B. fragilis* cell, thus allowing for its growth in the presence of these porphyrins.⁴⁶ We did not examine the HmuY homolog expressed by *B. thetaiotamicron* (termed Bth), but based on the high similarity of this protein to *B. fragilis* BfrA, we assumed similar heme-binding properties.

According to our hypothesis, although general structures of all hemophore-like proteins so far examined are similar, differences observed in heme-binding pockets or their surrounding loops result in different porphyrin-binding properties. Worth noting is the structure of BfrC protein, where a long α helix protrudes from the potential heme-binding pocket, which might prevent heme and PPIX binding. Although three-dimensional structures of all three Bfr apo-proteins are now known, the lack of knowledge of their structures in complex with heme/PPIX prevents us from confidently determining which amino acids are engaged in heme iron coordination in BfrA or which amino acids are responsible for PPIX binding to BfrB. Our mutational and spectroscopic analyses demonstrated that BfrB may preferentially bind PPIX, without heme iron coordination. Therefore, we assume that the function of BfrB could be similar to another *P. gingivalis* hemophore-like protein, namely, HusA, which binds PPIX,^{109,133} although with lower ability compared to BfrB (this study). Interestingly, we found that BfrB may also bind CPIII, one of the coproporphyrin isomers, possessing four propionates and therefore being different from PPIX, which has two propionate and two vinyl groups. CPIII can be found in the gut, and at higher levels in some human diseases such as porphyrias.¹³⁴ However, the possibility of whether CPIII could be used in vivo by *B. fragilis* instead of heme requires further elucidation since this compound did not support *B. fragilis* growth under in vitro conditions used in our study.

The colon niche and colonic mucosa exhibit an anaerobic environment,¹³⁵ allowing survival of both *P. gingivalis* and *B. fragilis*. However, an oxygen gradient exists not only along the human gastrointestinal tract but also across the intestinal wall.^{136,137} Being an anaerobic, asaccharolytic,

and highly proteolytic species, *P. gingivalis* may degrade the mucins and extracellular matrix components in the colon, infiltrate the mucus layer, invade the mucosa, and degrade immunological factors, resulting in increased potential for local and systemic inflammation. Deeper layers of the intestinal wall are generally normoxic.^{138,139} Therefore, HmuY, regardless of redox conditions, could be beneficial in heme binding, as compared to BfrA, enabling better growth and virulence of *P. gingivalis*, and thus reducing the abundance of *B. fragilis*, which might contribute to dysbiosis in the gut microbiome.

We demonstrated that *P. gingivalis* HmuY, functioning as a hemophore-like protein, can sequester heme from methemoglobin directly,⁶⁹ similar to classical bacterial hemophores, which are secreted proteins engaged in heme transfer from the host hemoproteins to the outer membrane receptors.^{140,141} HmuY is also able to compete with albumin, which is the normal front-line heme scavenger in vivo,⁶⁹ as well as acquiring heme from serum hemopexin.⁷³ Due to the excess of albumin, heme is first bound to albumin and then transferred to hemopexin.¹¹¹ Hemopexin is the serum heme-binding protein with the highest affinity for heme ($K_d \sim 10^{-13}$ - 10^{-10} M),^{113,142} which allows efficient heme extraction from human serum albumin ($K_d \sim 10^{-7}$ - 10^{-8} M).⁹⁰ Here, we found that only BfrA was able to capture heme bound to serum albumin, and only under reducing conditions, which is in accordance with similar properties of *T. forsythia* Tfo, *P. intermedia* PinO and PinA, and *B. vulgatus* Bvu.^{73,74,76} This effect could be explained by the lower affinity of albumin for Fe(II)heme compared to Fe(III)heme,^{114,115} which may facilitate heme capture by BfrA. The reducing conditions would also influence the properties of iron coordination by methionine residues more effectively compared to histidine residues, demonstrating that Met-ligand binding in the BfrA protein would be destabilized under oxidizing conditions.^{143,144} In contrast to HmuY homologs characterized so far, *P. gingivalis* HmuY can efficiently sequester heme from the albumin-heme complex under both air (oxidizing) and reducing conditions.^{69,73} Possible competition in heme acquisition between *P. gingivalis* and *B. fragilis* could be suggested, at least in part, by the fact that HmuY efficiently captured Fe(III)heme which had been bound to BfrA and BfrB. Based on these results, we conclude that heme bound to BfrA and BfrB might represent a heme reservoir for *P. gingivalis*, thus increasing this pathogen's virulence.

5 | CONCLUSIONS

Here, we report that *B. fragilis* expresses a heme-binding protein, BfrA, with properties of hemophore-like

proteins, which adds to the increasing number of members of the novel HmuY family. Importantly, our analysis confirms that various members of this family may have developed specific heme-binding pockets and the ability to sequester heme from host hemoproteins or even to acquire heme bound to heme-binding proteins produced by cohabitating bacteria. The independent evolution of these properties has resulted in different mechanisms of heme iron coordination in HmuY versus BfrA. HmuY binds heme very effectively both in oxidizing and reducing environments, while BfrA appears to prefer reducing conditions which would be encountered in the lower gut. In contrast, the second potential member of the HmuY family produced by *B. fragilis*, BfrB, prefers the binding of iron-free porphyrins. Although BfrC is structurally similar to HmuY and its homologs characterized so far, the protein is able to bind neither heme nor PPIX.

Our findings further demonstrate that the HmuY protein may compete with other members of the HmuY family to increase *P. gingivalis* virulence and its ability to also contribute to dysbiosis in the gut microbiome. We observed that BfrA and other HmuY homologs may bind heme, but importantly they may provide the HmuY protein with heme. Therefore, we assume that *P. gingivalis* HmuY might be superior in heme sequestration when *P. gingivalis* invades the gut microbiome. Further clarification of this mechanism is important because of the need to characterize one of the basic mechanisms that allow the survival of pathogens in the hostile environment of the host and that play a key role in dysbiosis, especially during the course of infections accompanying inflammatory systemic diseases. In addition, understanding the mechanisms that regulate this process could enable development of novel therapeutic approaches that are designed to control chronic inflammatory processes in both microbiomes. In this respect, our current experiments comprise construction and analysis of *B. fragilis* mutant strains lacking respective *bfr* genes to assess their importance in *B. fragilis* virulence.

AUTHOR CONTRIBUTIONS

Teresa Olczak, Svetlana V. Antonyuk, and Michał Śmiga were responsible for conceptualization. Svetlana V. Antonyuk, Klaudia Siemińska, Michał Śmiga, Richard W. Strange, Mateusz Wagner, and Katie J. Barnett performed experiments and collect the data. Svetlana V. Antonyuk, Klaudia Siemińska, Michał Śmiga, Richard W. Strange, and Teresa Olczak were responsible for data visualization and analysis. Teresa Olczak and Svetlana V. Antonyuk were responsible for funding acquisition, resources, and project administration. Teresa Olczak and Svetlana V. Antonyuk wrote the original manuscript. All authors contributed to reviewing and editing of the final manuscript.

ACKNOWLEDGMENTS

We thank the staff of the Diamond Light Source and the members of the University of Liverpool Molecular Biophysics Group for assistance with data collection. We would like to thank the staff and management of the Diamond Light Source, especially the staff of beamline I24, for their help and smooth operation of the facility. We thank Dr. John W. Smalley for the critical reading of the manuscript and very helpful comments. We also thank Richard Ashcroft for the English correction.

FUNDING INFORMATION

This study was funded by grant number 2019/33/B/NZ6/00292 from the National Science Center (Narodowe Centrum Nauki, NCN, Krakow, Poland) (to T.O.). The Diamond Light Source was accessed via the University of Liverpool BAG (proposal mx21970) (to S.V.A.).

DISCLOSURES

The authors have declared that no competing interests exist.

DATA AVAILABILITY STATEMENT

All relevant data are within the paper and in Supporting information, have been deposited in the RCSB PDB database under accession numbers 8B6A and 8B61, or are available upon request from the corresponding authors.

ORCID

Teresa Olczak  <https://orcid.org/0000-0002-6140-8144>

REFERENCES

1. Bashan A, Gibson TE, Friedman J, et al. Universality of human microbial dynamics. *Nature*. 2016;534:259-262. doi:10.1038/nature18301
2. Li K, Bihan M, Yooseph S, Methe BA. Analyses of the microbial diversity across the human microbiome. *PLoS ONE*. 2012;7(6):e32118. doi:10.1371/journal.pone.0032118
3. Takiishi T, Fenero CI, Camara NO. Intestinal barrier and gut microbiota: shaping our immune response throughout life. *Tissue Barriers*. 2017;5(4):e1373208. doi:10.1080/21688370.2017.1373208
4. Lamont RJ, Koo H, Hajishengallis G. The oral microbiota: dynamic communities and host interactions. *Nat Rev Microbiol*. 2018;16:745-759. doi:10.1038/s41579-018-0089-x
5. Gilbert JA, Blaser MJ, Caporaso JG, Jansson JK, Lynch SV, Knight R. Current understanding of the human microbiome. *Nat Med*. 2018;24:392-400. doi:10.1038/nm.4517
6. Zafar H, Sailer MH Jr. Gut *Bacteroides* species in health and disease. *Gut Microbes*. 2021;13(1):e1848158. doi:10.1080/19490976.2020.1848158
7. Mazmanian SK, Round JL, Kasper DL. A microbial symbiosis factor prevents intestinal inflammatory disease. *Nature*. 2008;453:620-625. doi:10.1038/nature07008

8. Kraal L, Abubucker S, Kota K, Fischbach MA, Mitreva M. The prevalence of species and strains in the human microbiome: a resource for experimental efforts. *PLoS ONE*. 2014;9(5):e97279. doi:10.1371/journal.pone.0097279
9. Bjursell MK, Martens EC, Gordon JJ. Functional genomic and metabolic studies of the adaptations of a prominent adult human gut symbiont, *Bacteroides thetaiotaomicron*, to the suckling period. *J Biol Chem*. 2006;281:36269-36279. doi:10.1074/jbc.M606509200
10. Wexler HM. *Bacteroides*: the good, the bad, and the nitty-gritty. *Clin Microbiol Rev*. 2007;20:593-621. doi:10.1128/CMR.00008-07
11. Vancamelbeke M, Vermeire S. The intestinal barrier: a fundamental role in health and disease. *Expert Rev Gastroenterol Hepatol*. 2017;11:821-834. doi:10.1080/17474124.2017.1343143
12. Baumgart DC, Carding SR. Inflammatory bowel disease: cause and immunobiology. *Lancet*. 2007;369:1627-1640. doi:10.1016/S0140-6736(07)60750-8
13. Bostanci N, Belibasakis GN. *Porphyromonas gingivalis*: an invasive and evasive opportunistic pathogen. *FEMS Microbiol Lett*. 2012;333:1-9. doi:10.1111/j.1574-6968.2012.02579.x
14. Darveau RP, Hajishengallis G, Curtis MA. *Porphyromonas gingivalis* as a potential community activist for disease. *J Dent Res*. 2012;91:816-820. doi:10.1177/0022034512453589
15. Hajishengallis G, Diaz PI. *Porphyromonas gingivalis*: immune subversion activities and role in periodontal dysbiosis. *Curr Oral Health Rep*. 2020;7:12-21. doi:10.1007/s40496-020-00249-3
16. Bregaint S, Boyer E, Fong SB, Meuric V, Bonnaure-Mallet M, Jolivet-Gougeon A. *Porphyromonas gingivalis* outside the oral cavity. *Odontologia*. 2022;110:1-19. doi:10.1007/s10266-021-00647-8
17. Llambes F, Arias-Herrera S, Caffesse R. Relationship between diabetes and periodontal infection. *World J Diabetes*. 2015;6:927-935. doi:10.4239/wjdv.v6.i7.927
18. Bansal M, Khatri M, Taneja V. Potential role of periodontal infection in respiratory diseases – a review. *J Med Life*. 2013;6:244-248.
19. Kashiwagi Y, Aburaya S, Sugiyama N, et al. *Porphyromonas gingivalis* induces entero-hepatic metabolic derangements with alteration of gut microbiota in a type 2 diabetes mouse model. *Sci Rep*. 2021;11(1):18398. doi:10.1038/s41598-021-97868-2
20. Dominy SS, Lynch C, Ermini F, et al. *Porphyromonas gingivalis* in Alzheimer's disease brains: evidence for disease causation and treatment with small-molecule inhibitors. *Sci Adv*. 2019;5(1):eaau3333. doi:10.1126/sciadv.aau3333
21. Aguayo S, Schuh CMAP, Vicente B, Aguayo LG. Association between Alzheimer's disease and oral and gut microbiota: are pore forming proteins the missing link? *J Alzheimers Dis*. 2018;65:29-46. doi:10.3233/JAD-180319
22. Mei F, Xie M, Huang X, et al. *Porphyromonas gingivalis* and its systemic impact: current status. *Pathogens*. 2020;9(11):944. doi:10.3390/pathogens9110944
23. Olsen I, Yamazaki K. Can oral bacteria affect the microbiome of the gut? *J Oral Microbiol*. 2019;11(1):1586422. doi:10.1080/20002297.2019.1586422
24. Schmidt TS, Hayward MR, Coelho LP, et al. Extensive transmission of microbes along the gastrointestinal tract. *Elife*. 2019;8:e42693. doi:10.7554/eLife.42693
25. Kato T, Yamazaki K, Nakajima M, et al. Oral administration of *Porphyromonas gingivalis* alters the gut microbiome and serum metabolome. *mSphere*. 2018;3(5):e00460-18. doi:10.1128/mSphere.00460-18
26. Hamamoto Y, Ouhara K, Munenaga S, et al. Effect of *Porphyromonas gingivalis* infection on gut dysbiosis and resultant arthritis exacerbation in mouse model. *Arthritis Res Ther*. 2020;22(1):249. doi:10.1186/s13075-020-02348-z
27. Kobayashi R, Ogawa Y, Hashizume-Takizawa T, Kurita-Ochiai T. Oral bacteria affect the gut microbiome and intestinal immunity. *Pathog Dis*. 2020;78(3):ftaa024. doi:10.1093/femspd/ftaa024
28. du Teil EM, Gabarrini G, Harmsen HJM. Talk to your gut: the oral-gut microbiome axis and its immunomodulatory role in the etiology of rheumatoid arthritis. *FEMS Microbiol Rev*. 2018;43:1-18. doi:10.1093/femsre/fuy035
29. Arimatsu K, Yamada H, Miyazawa H, et al. Oral pathobiont induces systemic inflammation and metabolic changes associated with alteration of gut microbiota. *Sci Rep*. 2014;4:4828. doi:10.1038/srep04828
30. Simas AM, Kramer CD, Weinberg EO, Genco CA. Oral infection with a periodontal pathogen alters oral and gut microbiomes. *Anaerobe*. 2021;71:102399. doi:10.1016/j.anaerobe.2021.102399
31. Read E, Curtis MA, Neves JF. The role of oral bacteria in inflammatory bowel disease. *Nat Rev Gastroenterol Hepatol*. 2021;18:731-742. doi:10.1038/s41575-021-00488-4
32. Seedorf H, Griffin NW, Ridaura VK, et al. Bacteria from diverse habitats colonize and compete in the mouse gut. *Cell*. 2014;159:253-266. doi:10.1016/j.cell.2014.09.008
33. Sato K, Takahashi N, Kato T, et al. Aggravation of collagen-induced arthritis by orally administered *Porphyromonas gingivalis* though modulation of the gut microbiota and gut immune system. *Sci Rep*. 2017;1:6955. doi:10.1038/s41598-017-07196-7
34. Kramer CD, Simas AM, He X, Ingalla RR, Weinberg EO, Genco CA. Distinct roles for dietary lipids and *Porphyromonas gingivalis* infection on atherosclerosis progression and the gut microbiota. *Anaerobe*. 2017;45:19-30. doi:10.1016/j.anaerobe.2017.04.011
35. Dong ZJ, Lv WQ, Zhang CY, Chen S. Correlation analysis of gut microbiota and serum metabolome with *Porphyromonas gingivalis*-induced metabolic disorders. *Front Cell Infect Microbiol*. 2022;12:858902. doi:10.3389/fcimb.2022.858902
36. Tsuzuno T, Takahashi N, Yamada-Hara M, et al. Ingestion of *Porphyromonas gingivalis* exacerbates colitis via intestinal epithelial barrier disruption in mice. *J Periodontol Res*. 2021;56:275-288. doi:10.1111/jre.12816
37. Segata N, Haake SK, Mannon P, et al. Composition of the adult digestive tract bacterial microbiome based on seven mouth surfaces, tonsils, throat and stool samples. *Genome Biol*. 2012;13(6):R42. doi:10.1186/gb-2012-13-6-r42
38. Papageorgiou SN, Hagner M, Nogueira AV, Franke A, Jager A, Deschner J. Inflammatory bowel disease and oral health: systematic review and a meta-analysis. *J Clin Periodontol*. 2017;44:382-393. doi:10.1111/jcpe.12698
39. Lee YC, Liu CY, Lee CL, Zhang RH, Huang CJ, Yen TL. The periodontopathic pathogen, *Porphyromonas gingivalis*, involves a gut inflammatory response and exacerbates inflammatory bowel disease. *Pathogens*. 2021;11(1):84. doi:10.3390/pathogens11010084
40. Kabeerdoss J, Jayakanthan P, Pugazhendhi S, Ramakrishna BS. Alterations of mucosal microbiota in the colon of patients with inflammatory bowel disease revealed by real time

- polymerase chain reaction amplification of 16S ribosomal ribonucleic acid. *Indian J Med Res.* 2015;142:23-32. doi:10.4103/0971-5916.162091
41. Bibiloni R, Mangold M, Madsen KL, Fedorak RN, Tannock GW. The bacteriology of biopsies differs between newly diagnosed, untreated, Crohn's disease and ulcerative colitis patients. *J Med Microbiol.* 2006;55:1141-1149. doi:10.1099/jmm.0.46498-0
 42. Zhao X, Liu J, Zhang C, et al. *Porphyromonas gingivalis* exacerbates ulcerative colitis via *Porphyromonas gingivalis* peptidylarginine-deiminase. *Int J Oral Sci.* 2021;13(1):31. doi:10.1038/s41368-021-00136-2
 43. Dailey HA, Dailey TA, Gerdes S, et al. Prokaryotic heme biosynthesis: pathways to a common essential product. *Microbiol Mol Biol Rev.* 2017;81(1):e00048-16. doi:10.1128/MMBR.00048-16
 44. Sperry JF, Appleman MD, Wilkins TD. Requirement of heme for growth *Bacteroides fragilis*. *Appl Environ Microbiol.* 1977;34:386-390. doi:10.1128/aem.34.4.386-390.1977
 45. Rocha ER, de Uzeda M, Brock JH. Effect of ferric and ferrous iron chelators on growth of *Bacteroides fragilis* under anaerobic conditions. *FEMS Microbiol Lett.* 1991;84:45-50. doi:10.1016/0378-1097(91)90393-o
 46. Rocha ER, Bergonia HA, Gerdes S, Smith CJ. *Bacteroides fragilis* requires the ferrous-iron transporter FeoAB and the CobN-like proteins BtuS1 and BtuS2 for assimilation of iron released from heme. *MicrobiologyOpen.* 2019;8(4):e00669. doi:10.1002/mbo3.669
 47. Rocha ER, Smith CJ. Heme and iron metabolism in *Bacteroides*. In: Andrews SC, Cornelis P, eds. *Iron uptake and homeostasis in microorganisms*. Caister Academic Press; 2010:153-165.
 48. Olczak T, Maszczak-Seneczko D, Smalley JW, Olczak M. Gallium(III), cobalt(III) and copper(II) protoporphyrin IX exhibit antimicrobial activity against *Porphyromonas gingivalis* by reducing planktonic and biofilm growth and invasion of host epithelial cells. *Arch Microbiol.* 2012;194:719-724. doi:10.1007/s00203-012-0804-3
 49. Fyrestam J, Bjurshammar N, Paulsson E, Johannsen A, Ostman C. Determination of porphyrins in oral bacteria by liquid chromatography electrospray ionization tandem mass spectrometry. *Anal Bioanal Chem.* 2015;407:7013-7023. doi:10.1007/s00216-015-8864-2
 50. Fyrestam J, Bjurshammar N, Paulsson E, Mansouri N, Johannsen A, Ostman C. Influence of culture conditions on porphyrin production in *Aggregatibacter actinomycetemcomitans* and *Porphyromonas gingivalis*. *Photodiagnosis Photodyn Ther.* 2017;17:115-123. doi:10.1016/j.pdpdt.2016.11.001
 51. Fuller MD, Caldwell DR. Tetrapyrrole utilization of *Bacteroides fragilis*. *Can J Microbiol.* 1982;28:1304-1310. doi:10.1139/m82-195
 52. Rodionov DA, Vitreschak AG, Mironov AA, Gelfand MS. Comparative genomics of the vitamin B12 metabolism and regulation in prokaryotes. *J Biol Chem.* 2003;278:41148-41159. doi:10.1074/jbc.M305837200
 53. Roper JM, Raux E, Brindley AA, et al. The enigma of cobalamin (vitamin B12) biosynthesis in *Porphyromonas gingivalis*. Identification and characterization of a functional corrin pathway. *J Biol Chem.* 2000;275:40316-40323. doi:10.1074/jbc.M007146200
 54. Olczak T, Simpson W, Liu X, Genco CA. Iron and heme utilization in *Porphyromonas gingivalis*. *FEMS Microbiol Rev.* 2005;29:119-144. doi:10.1016/j.femsre.2004.09.001
 55. Olczak T, Sroka A, Potempa J, Olczak M. *Porphyromonas gingivalis* HmuY and HmuR: further characterization of a novel mechanism of heme utilization. *Arch Microbiol.* 2008;189:197-210. doi:10.1007/s00203-007-0309-7
 56. Parker AC, Bergonia HA, Seals NL, Baccanale CL, Rocha ER. The *uroS* and *yifB* genes conserved among tetrapyrrole synthesizing-deficient *Bacteroidales* are involved in *Bacteroides fragilis* heme assimilation and survival in experimental intra-abdominal infection and intestinal colonization. *Infect Immun.* 2020;88(8):e00103-20. doi:10.1128/IAI.00103-20
 57. Zhu W, Winter MG, Spiga L, et al. Xenosiderophore utilization promotes *Bacteroides thetaiotaomicron* resilience during colitis. *Cell Host Microbe.* 2020;27:376-388. doi:10.1016/j.chom.2020.01.010
 58. Rocha ER, Krykunivsky AS. Anaerobic utilization of Fe(III)-xenosiderophores among *Bacteroides* species and the distinct assimilation of Fe(III)-ferrichrome by *Bacteroides fragilis* within the genus. *MicrobiologyOpen.* 2017;16(4):e00479. doi:10.1002/mbo3.479
 59. Dashper SG, Butler CA, Lissel JP, et al. A novel *Porphyromonas gingivalis* FeoB plays a role in manganese accumulation. *J Biol Chem.* 2005;280:28095-28102. doi:10.1074/jbc.M503896200
 60. Otto BR, Verweij-van Vught AM, van Doorn J, MacLaren DM. Outer membrane proteins in *Bacteroides fragilis* and *Bacteroides vulgatus* in relation to iron uptake and virulence. *Microb Pathog.* 1988;4:279-287. doi:10.1016/0882-4010(88)90088-5
 61. Veeranagouda Y, Husain F, Boente R, et al. Deficiency of the ferrous iron transporter FeoAB is linked with metronidazole resistance in *Bacteroides fragilis*. *J Antimicrob Chemother.* 2014;69:2634-2643. doi:10.1093/jac/dku219
 62. Otto BR, Sparrius M, Verweij-van Vught AM, MacLaren DM. Iron-regulated outer membrane protein of *Bacteroides fragilis* involved in heme uptake. *Infect Immun.* 1990;58(12):3954-3958.
 63. Otto BR, Verweij WR, Sparrius M, Verweij-van Vught AMJJ, Nord CE, MacLaren DM. Human immune response to an iron-repressible outer membrane protein of *Bacteroides fragilis*. *Infect Immun.* 1991;59:2999-3003. doi:10.1128/iai.59.9.2999-3003.1991
 64. Otto BR, Sparrius M, Worst DJ, de Graaf FK, MacLaren DM. Utilization of haem from the haptoglobin-haemoglobin complex by *Bacteroides fragilis*. *Microb Pathog.* 1994;17:137-147. doi:10.1006/mpat.1994.1060
 65. Otto BR, Kusters JG, Luirink J, De Graaf FK, Oudega B. Molecular characterization of a heme-binding protein of *Bacteroides fragilis* BE1. *Infect Immun.* 1996;64:4345-4350. doi:10.1128/iai.64.10.4345-4350.1996
 66. Lobo LA, Jenkins AL, Smith CJ, Rocha ER. Expression of *Bacteroides fragilis* hemolysins *in vivo* and role of HlyBA in an intra-abdominal infection model. *MicrobiologyOpen.* 2013;2:326-327. doi:10.1002/mbo3.76
 67. Robertson KP, Smith CJ, Gough AM, Rocha ER. Characterization of *Bacteroides fragilis* hemolysins and regulation and synergistic interactions of HlyA and HlyB. *Infect Immun.* 2006;74:2304-2316. doi:10.1128/IAI.74.4.2304-2316.2006
 68. Smalley JW, Olczak T. Haem acquisition mechanisms of *Porphyromonas gingivalis*—strategies used in polymicrobial community in a haem-limited host environment. *Mol Oral Microbiol.* 2017;32:1-23. doi:10.1111/omi.12149
 69. Smalley JW, Byrne DP, Birss AJ, et al. HmuY haemophore and gingipain proteases constitute a unique syntrophic system of

- haem acquisition by *Porphyromonas gingivalis*. *PLoS ONE*. 2011;6(2):e17182. doi:10.1371/journal.pone.0017182
70. Byrne DP, Potempa J, Olczak T, Smalley JW. Evidence of mutualism between two periodontal pathogens: co-operative haem acquisition by the HmuY haemophore of *Porphyromonas gingivalis* and the cysteine protease interpain A (InpA) of *Prevotella intermedia*. *Mol Oral Microbiol*. 2013;28:219-229. doi:10.1111/omi.12018
 71. Brown JL, Yates EA, Bielecki M, Olczak T, Smalley JW. Potential role for *Streptococcus gordonii*-derived hydrogen peroxide in heme acquisition by *Porphyromonas gingivalis*. *Mol Oral Microbiol*. 2018;33:322-335. doi:10.1111/omi.12229
 72. Benedyk M, Byrne DP, Glowczyk I, et al. Pyocyanin: a contributory factor in haem acquisition and virulence enhancement of *Porphyromonas gingivalis* in the lung. *PLoS ONE*. 2015;10(2):e0118319. doi:10.1371/journal.pone.0118319
 73. Bielecki M, Antonyuk S, Strange RW, et al. *Tannerella forsythia* Tfo belongs to *Porphyromonas gingivalis* HmuY-like family of proteins but differs in heme-binding properties. *Biosci Rep*. 2018;38(5):BSR20181325. doi:10.1042/BSR20181325
 74. Bielecki M, Antonyuk S, Strange RW, et al. *Prevotella intermedia* produces two proteins homologous to *Porphyromonas gingivalis* HmuY but with different heme coordination mode. *Biochem J*. 2020;477:381-405. doi:10.1042/BCJ20190607
 75. Slezak P, Smiga M, Smalley JW, Sieminska K, Olczak T. *Porphyromonas gingivalis* HmuY and *Streptococcus gordonii* GAPDH – novel heme acquisition strategy in the oral microbiome. *Int J Mol Sci*. 2020;21:4150. doi:10.3390/ijms21114150
 76. Sieminska K, Cierpisz P, Smiga M, Olczak T. *Porphyromonas gingivalis* HmuY and *Bacteroides vulgatus* Bvu – a novel competitive heme acquisition strategy. *Int J Mol Sci*. 2021;22(5):2237. doi:10.3390/ijms22052237
 77. Olczak T, Sosicka P, Olczak M. HmuY is an important virulence factor for *Porphyromonas gingivalis* growth in the heme-limited host environment and infection of macrophages. *Biochem Biophys Res Commun*. 2015;467:48-753. doi:10.1016/j.bbrc.2015.10.070
 78. Deng ZL, Sztajer H, Jarek M, Bhujju S, Wagner-Dobler I. Worlds apart – transcriptome profiles of key oral microbes in the periodontal pocket compared to single laboratory culture reflect synergistic interactions. *Front Microbiol*. 2018;9:124. doi:10.1038/s41598-017-03804-8
 79. Trindade SC, Olczak T, Gomes-Filho IS, et al. Induction of interleukin (IL)-1 β , IL-10, IL-8 and immunoglobulin G by *Porphyromonas gingivalis* in humans. *J Periodontol Res*. 2012;47:27-32. doi:10.1111/j.1600-0765.2011.01401.x
 80. Smiga M, Sieminska K, Trindade SC, Gomes-Filho IS, Nobre dos Santos EK, Olczak T. Reactivity of serum IgG antibodies with hemophore-like proteins expressed by periodontopathogens: *Porphyromonas gingivalis* HmuY and *Prevotella intermedia* PinA as potential markers of periodontitis. *J Oral Microbiol*. 2023; 15:2214455. doi:10.1080/20002297.2023.2214455
 81. Smiga M, Bielecki M, Olczak M, Olczak T. *Porphyromonas gingivalis* PgFur is a member of a novel fur subfamily with non-canonical function. *Front Cell Infect Microbiol*. 2019;9:233. doi:10.3389/fcimb.2019.00233
 82. Smiga M, Slezak P, Wagner M, Olczak T. Interplay between *Porphyromonas gingivalis* hemophore-like protein HmuY and Kgp/RgpA gingipains plays a superior role in heme supply. *Microbiol Spectr*. 2023;11(2):e0459322. doi:10.1128/spectrum.04593-22
 83. Wojtowicz H, Guevara T, Tallant C, et al. Unique structure and stability of HmuY, a novel heme-binding protein of *Porphyromonas gingivalis*. *PLoS Pathog*. 2009;5(5):e1000419. doi:10.1371/journal.ppat.1000419
 84. Wojtowicz H, Wojaczynski J, Olczak M, Krolczewski J, Latos-Grazynski L, Olczak T. Heme environment of *Porphyromonas gingivalis* HmuY heme-binding protein. *Biochem Biophys Res Commun*. 2009;382:178-182. doi:10.1016/j.bbrc.2009.03.148
 85. Wojaczynski J, Wojtowicz H, Bielecki M, et al. Iron(III) mesoporphyrin IX and iron(III) deuteroporphyrin IX bind to the *Porphyromonas gingivalis* HmuY hemophore. *Biochem Biophys Res Commun*. 2011;411:299-304. doi:10.1016/j.bbrc.2011.06.129
 86. Wojtowicz H, Bielecki M, Wojaczynski J, Olczak M, Smalley JW, Olczak T. *Porphyromonas gingivalis* HmuY haemophore binds gallium(III), zinc(II), cobalt(III), manganese(III), nickel(II), and copper(II) protoporphyrin IX but in a manner different to iron(III) protoporphyrin IX. *Metallomics*. 2013;5:343-351. doi:10.1039/c3mt20215a
 87. Vall-Sagarra A, McMicken B, Nonell S, Brancalione L. Effects of visible-light irradiation of protoporphyrin IX on the self-assembly of tubulin heterodimers. *ChemPhysChem*. 2016;17:3269-3282. doi:10.1002/cphc.201600629
 88. Gabler T, Sebastiani F, Helm J, et al. Substrate specificity and complex stability of coproporphyrin ferrochelatase is governed by hydrogen-bonding interactions of the four propionate groups. *FEBS J*. 2022;289:1680-1699. doi:10.1111/febs.16257
 89. Winter G, Waterman DG, Parkhurst JM, et al. DIALS: implementation and evaluation of a new integration package. *Acta Crystallogr D Struct Biol*. 2018;74(Pt2):85-97. doi:10.1107/S2059798317017235
 90. Evans PR, Murshudov GN. How good are my data and what is the resolution? *Acta Crystallogr D Biol Crystallogr*. 2013;69(Pt7):1204-1214. doi:10.1107/S090744491300006
 91. Winn MD, Ballard CC, Cowtan KD, et al. Overview of the CCP4 suite and current developments. *Acta Crystallogr D Biol Crystallogr*. 2011;67(Pt 4):235-242. doi:10.1107/S0907444910045749
 92. Vagin A, Teplyakov A. Molecular replacement with MOLREP. *Acta Crystallogr D Biol Crystallogr*. 2010;66(Pt1):22-25. doi:10.1107/S0907444909042589
 93. Chojnowski G, Choudhury K, Heuser P, et al. The use of local structural similarity of distant homologues for crystallographic model building from a molecular-replacement solution. *Acta Crystallogr D Struct Biol*. 2020;76:248-260. doi:10.1107/S2059798320000455
 94. Emsley P, Lohkamp B, Scott WG, Cowtan K. Features and development of coot. *Acta Crystallogr D Biol Crystallogr*. 2010;66(Pt 4):486-501. doi:10.1107/S0907444910007493
 95. Murshudov GN, Skubak P, Lebedev AA, et al. REFMAC5 for the refinement of macromolecular crystal structures. *Acta Crystallogr D Biol Crystallogr*. 2011;67(Pt 4):355-367. doi:10.1107/S0907444911001314
 96. Abraham MJ, Murtola T, Schulz R, et al. GROMACS: high performance molecular simulations through multi-level parallelism from laptops to supercomputers. *SoftwareX*. 2015;1:19-25. doi:10.1016/j.softx.2015.06.001
 97. Schmid N, Eichenberger A, Choutko A, et al. Definition and testing of the GROMOS force-field versions 54A7

- and 54B7. *Eur Biophys J*. 2011;40:843-856. doi:10.1007/s00249-011-0700-9
98. Berendsen HJC, Postma JPM, van Gunsteren WF, Hermans J. Intermolecular Forces. In: Pullman B, ed. *Interaction Models for Water in Relation to Protein Hydration*. Reidel; 1981:331-342.
 99. Parrinello M, Rahman A. Polymorphic transitions in single crystals: a new molecular dynamics method. *J Appl Phys*. 1981;52:7182-7190. doi:10.1063/1.328693
 100. Essmann U, Perera L, Berkowitz ML, Darden T, Lee H, Pedersen LG. A smooth particle mesh Ewald method. *J Chem Phys*. 1995;103:8577-8593. doi:10.1063/1.470117
 101. Humphrey W, Dalke A, Schulten K. VMD—visual molecular dynamics. *J Mol Graph*. 1996;14:33-38. doi:10.1016/0263-7855(96)00018-5
 102. Madeira F, Park YM, Lee J, et al. The EMBL-EBI search and sequence analysis tools APIs in 2019. *Nucleic Acids Res*. 2019;47(W1):W636-W641. doi:10.1093/nar/gkz268
 103. Pettersen EF, Goddard TD, Huang CC, Meng EC, Couch GS, Croll TI. UCSF ChimeraX: structure visualization for researchers, educators, and developers. *Protein Sci*. 2021;30:70-82. doi:10.1002/pro.3943
 104. Jumper J, Evans R, Pritzel A, et al. Highly accurate protein structure prediction with AlphaFold. *Nature*. 2021;596:583-589. doi:10.1038/s41586-021-03819-2
 105. Varadi M, Anyango S, Deshpande M, et al. AlphaFold protein structure database: massively expanding the structural coverage of protein-sequence space with high-accuracy models. *Nucleic Acids Res*. 2022;50(D1):D439-D444. doi:10.1093/nar/gkab1061
 106. Guex N, Peitsch MC. SWISS-MODEL and the Swiss-PdbViewer: an environment for comparative protein modeling. *Electrophoresis*. 1997;18:2714-2723. doi:10.1002/elps.1150181505
 107. Liu X, Olczak T, Guo HC, Dixon DW, Genco CA. Identification of amino acid residues involved in heme binding and hemo-protein utilization in the *Porphyromonas gingivalis* heme receptor HmuR. *Infect Immun*. 2006;74:1222-1232. doi:10.1128/IAI.74.2.1222-1232.2006
 108. Olczak T. Analysis of conserved glutamate residues in *Porphyromonas gingivalis* outer membrane receptor HmuR: toward a further understanding of heme uptake. *Arch Microbiol*. 2006;186:393-402. doi:10.1007/s00203-006-0151-3
 109. Gao JL, Kwan AH, Yammine A, et al. Structural properties of a haemophore facilitate targeted elimination of the pathogen *Porphyromonas gingivalis*. *Nat Commun*. 2018;9(1):4097. doi:10.1038/s41467-018-06470-0
 110. Morgan WT. The binding and transport of heme by hemopexin. *Ann Clin Res*. 1976;8:223-232.
 111. Morgan WT, Liem HH, Sutor RP, Muller-Eberhard U. Transfer of heme from heme-albumin to hemopexin. *Biochim Biophys Acta*. 1976;444:435-445. doi:10.1016/0304-4165(76)90387-1
 112. Paoli M, Anderson BF, Baker HM, Morgan WT, Smith A, Baker EN. Crystal structure of hemopexin reveals a novel high-affinity heme site formed between two beta-propeller domains. *Nat Struct Biol*. 1999;6:926-931. doi:10.1038/13294
 113. Detzel MS, Schmalohr BF, Steinbock F, et al. Revisiting the interaction of heme hemopexin. *Biol Chem*. 2021;402:675-691. doi:10.1515/hsz-2020-0347
 114. Cao Y, Nicoletti FP, De Sanctis G, et al. Evidence for pH-dependent multiple conformers in iron(II) heme-human serum albumin: spectroscopic and kinetic investigation of carbon monoxide binding. *J Biol Inorg Chem*. 2012;17:133-147. doi:10.1007/s00775-011-0837-0
 115. Bocedi A, De Sanctis G, Ciaccio C, et al. Reciprocal allosteric modulation of carbon monoxide and warfarin binding to ferrous human serum heme-albumin. *PLoS ONE*. 2013;8:e58842. doi:10.1371/journal.pone.0058842
 116. Hanna DA, Harvey RM, Martinez-Guzman O, et al. Heme dynamics and trafficking factors revealed by genetically encoded fluorescent heme sensors. *Proc Natl Acad Sci U S A*. 2016;113:7539-7544. doi:10.1073/pnas.1523802113
 117. Yuan X, Rietzschel N, Kwon H, et al. Regulation of intracellular heme trafficking revealed by subcellular reporters. *Proc Natl Acad Sci U S A*. 2016;113:E5144-E5152. doi:10.1073/pnas.1609865113
 118. Hooda J, Shah A, Zhang L. Heme, an essential nutrient from dietary proteins, critically impacts diverse physiological and pathological processes. *Nutrients*. 2014;6:1080-1102. doi:10.3390/nu6031080
 119. West AR, Oates PS. Mechanisms of heme iron absorption: current questions and controversies. *World J Gastroenterol*. 2008;14:4101-4110. doi:10.1111/j.1365-2958.2012.08136.x
 120. Ijssennagger N, Belzer C, Hooiveld GJ, et al. Gut microbiota facilitates dietary heme-induced epithelial hyperproliferation by opening the mucus barrier in colon. *Proc Natl Acad Sci U S A*. 2015;112:10038-10043. doi:10.1073/pnas.1507645112
 121. Ijssennagger N, Derrien M, van Doorn GM, et al. Dietary heme alters microbiota and mucosa of mouse colon without functional changes in host-microbe cross-talk. *PLoS ONE*. 2012;7(12):e49868. doi:10.1371/journal.pone.0049868
 122. Otto BR, van Dooren SJ, Dozois CM, Luirink J, Oudega B. *Escherichia coli* hemoglobin protease autotransporter contributes to synergistic abscess formation and heme-dependent growth of *Bacteroides fragilis*. *Infect Immun*. 2002;70:5-10. doi:10.1128/IAI.70.1.5-10.2002
 123. Rocha ER, Smith A, Smith CJ, Brock JH. Growth inhibition of *Bacteroides fragilis* by hemopexin: proteolytic degradation of hemopexin to overcome heme limitation. *FEMS Microbiol Lett*. 2001;199:73-78. doi:10.1111/j.1574-6968.2001.tb10653.x
 124. Stojiljkovic I, Hantke K. Hemin uptake system of *Yersinia enterocolitica*: similarities with TonB-dependent systems in gram-negative bacteria. *EMBO J*. 1992;11:4359-4367. doi:10.1002/j.1460-2075.1992.tb05535.x
 125. Benevides-Matos N, Biville F. The hem and has haem uptake systems in *Serratia marcescens*. *Microbiology*. 2010;156:1749-1757. doi:10.1099/mic.0.034405-0
 126. Schauer K, Rodionov DA, de Reuse H. New substrates for TonB-dependent transport: do we only see the 'tip of the iceberg'? *Trends Biochem Sci*. 2008;33:330-338. doi:10.1016/j.tibs.2008.04.012
 127. Pollet RM, Martin LM, Koropatkin NM. TonB-dependent transporters in the Bacteroidetes: unique domain structures and potential functions. *Mol Microbiol*. 2021;115:490-501. doi:10.1111/mmi.14683
 128. Wilson MM, Anderson DE, Bernstein HD. Analysis of the outer membrane proteome and secretome of *Bacteroides fragilis* reveals a multiplicity of secretion mechanisms. *PLoS ONE*. 2015;10(2):e0117732. doi:10.1371/journal.pone.0117732
 129. Elhenawy W, Debely MO, Feldman MF. Preferential packing of acidic glycosidases and proteases into *Bacteroides* outer

- membrane vesicles. *MBio*. 2014;5(2):e00909-14. doi:10.1128/mBio.00909-14
130. Pierce JV, Fellows JD, Anderson DE, Bernstein HD. A clostripain-like protease plays a major role in generating the secretome of enterotoxigenic *Bacteroides fragilis*. *Mol Microbiol*. 2021;115:290-304. doi:10.1111/mmi.14616
131. Cerdeno-Tarraga AM, Patrick S, Crossman LC, et al. Extensive DNA inversions in the *B. fragilis* genome control variable gene expression. *Science*. 2005;307:1463-1465. doi:10.1126/science.1107008
132. Kosno J, Sieminska K, Olczak T. Unique properties of heme binding of the *Porphyromonas gingivalis* HmuY hemophore-like protein result from the evolutionary adaptation of the protein structure. *Molecules*. 2022;27(5):1703. doi:10.3390/molecules27051703
133. Gao JL, Nguyen KA, Hunter N. Characterization of a hemophore-like protein from *Porphyromonas gingivalis*. *J Biol Chem*. 2010;285:40028-40038. doi:10.1074/jbc.M110.163535
134. Kuhnel A, Gross U, Jacob K, Doss MO. Studies on coproporphyrin isomers in urine and feces in the porphyrias. *Clin Chim Acta*. 1999;282:45-55. doi:10.1016/s0009-8981(99)00036-4
135. Donaldson GP, Lee SM, Mazmanian SK. Gut biogeography of the bacterial microbiota. *Nat Rev Microbiol*. 2016;14:20-32. doi:10.1038/nrmicro3552
136. Espey M. Role of oxygen gradients in shaping redox relationship between the human intestine and its microbiota. *Free Radic Biol Med*. 2013;55:130-140. doi:10.1016/j.freeradbiomed.2012.10.554
137. Albenberg L, Esipova TV, Judge CP, et al. Correlation between intraluminal oxygen gradient and radial partitioning of intestinal microbiota in humans and mice. *Gastroenterology*. 2014;147:1055-1063. doi:10.1053/j.gastro.2014.07.020
138. Colgan SP, Campbell EL, Kominsky DJ. Hypoxia and mucosal inflammation. *Annu Rev Pathol*. 2016;11:77-100. doi:10.1146/annurev-pathol-012615-044231
139. Singhal R, Shah YM. Oxygen battle in the gut: hypoxia and hypoxia-inducible factors in metabolic and inflammatory responses in the intestine. *J Biol Chem*. 2020;295:10493-10505. doi:10.1074/jbc.REV120.011188
140. Benson DR, Rivera M. Heme uptake and metabolism in bacteria. *Met Ions Life Sci*. 2013;12:279-332. doi:10.1007/978-94-007-5561-1_9
141. Wandersman C, Delepelaire P. Haemophore functions revisited. *Mol Microbiol*. 2012;85:618-631.
142. Hrkal Z, Vodrazka Z, Kalousek I. Transfer of heme from ferrihemoglobin and ferrihemoglobin isolated chains to hemopexin. *Eur J Biochem*. 1974;43:73-78. doi:10.1111/j.1432-1033.1974.tb03386.x
143. Schejter A, Plotkin B, Vig I. The reactivity of cytochrome *c* with soft ligands. *FEBS Lett*. 1991;280:199-201. doi:10.1016/0014-5793(91)80292-b
144. Ayers PW, Parr RG, Pearson RG. Elucidating the hard/soft acid/base principle: a perspective based on half-reactions. *J Chem Phys*. 2006;124:194107. doi:10.1063/1.2196882

SUPPORTING INFORMATION

Additional supporting information can be found online in the Supporting Information section at the end of this article.

How to cite this article: Antonyuk SV, Siemińska K, Śmiga M, et al. *Bacteroides fragilis* expresses three proteins similar to *Porphyromonas gingivalis* HmuY: Hemophore-like proteins differentially evolved to participate in heme acquisition in oral and gut microbiomes. *The FASEB Journal*. 2023;37:e22981. doi:10.1096/fj.202300366R